buildings

MDPI

Article

From Vulnerability to Resilience: Passive Design Strategies for Optimizing Building Envelope Heat Exchange to Reduce Cooling Loads in a Warming World

Tao Ning [1], Junxue Zhang [1,*], Hairuo Wang [2] and Ge Song [3]

[1] School of Civil Engineering and Architecture, Jiangsu University of Science and Technology, Zhenjiang 212100, China
[2] School of Civil and Ocean Engineering, Jiangsu Ocean University, Lianyungang 222005, China
[3] Energy and Process Technology, Norwegian University of Science and Technology, 7034 Trondheim, Norway
* Correspondence: zjx2021@just.edu.cn

Abstract

Traditional air conditioning consumes substantial electricity, exacerbates the urban heat island effect, and creates a maladaptive feedback loop, necessitating a shift toward passive-first net-zero pathways. This study takes a typical six-story residential building in Nanjing's hot summer and cold winter climate zone as a case study. Using EnergyPlus hourly simulations, three progressive passive strategy packages are designed to quantify the impact of building envelope heat exchange on cooling loads, grid stress, and heat resilience. Package A includes external shading and natural ventilation. Package B adds reflective coating and a green roof. Package C further adds night ventilation precooling and high-performance windows. The results show that Package C achieves a 62.5% reduction in peak cooling load and a 63.0% reduction in seasonal cooling load. Daytime peak inward heat gain decreases from 68 W/m^2 to 22 W/m^2, while nighttime outward heat dissipation increases from 12 W/m^2 to 38 W/m^2. Under an extreme heat day of 41.2 °C with no active cooling, indoor peak temperature drops from 36.8 °C to 29.4 °C, and heat risk hours decrease by 73.6%. Peak-hour power demand is reduced by 70.4%, with a systemic leverage factor of 1.08. Innovations include achieving over 60% load reduction using only mature passive strategies, introducing the systemic leverage factor to quantify urban heat island mitigation benefits, and establishing a vulnerability-to-resilience transformation framework. The passive-first pathway validates building envelope as the first line of defense for net-zero futures. However, the findings are based on a typical six-story residential building in Nanjing and require validation through field measurements or broader application across different climate zones and building typologies before generalization.

Keywords: passive design strategy; envelope thermal performance; heat transfer; cooling load; net-zero pathway

Check for updates

Academic Editor: Apple L.S. Chan

Received: 24 May 2026
Revised: 19 June 2026
Accepted: 21 June 2026
Published: 24 June 2026

Copyright: © 2026 by the authors. Licensee MDPI, Basel, Switzerland. This article is an open access article distributed under the terms and conditions of the Creative Commons Attribution (CC BY) license.

1. Introduction

Global warming has led to a continuous increase in the frequency and intensity of extreme high-temperature weather, and the health risks related to high temperatures have also risen [1,2]. At the same time, the widespread use of traditional air conditioners has formed an unsuitable feedback loop: consuming a large amount of electricity, putting huge pressure on the power grid during peak hours, and further intensifying the urban heat island effect through waste heat emissions. Active mechanical cooling has evolved from a

convenience in life to a systemic vulnerability, and the net-zero emission path that solely relies on electrification faces severe challenges [3,4]. Against this backdrop, the design principle of passive priority is receiving increasing attention, i.e., by optimizing the heat exchange performance of the building envelope, the load is actively reduced before the mechanical system is activated, thereby enhancing the thermal autonomy and resilience of the building itself.

International academic research on passive building strategies has developed over several decades [5–7]. Europe, as a pioneer, saw the German Passive House Institute establish the Passive House standard in the 1990s, emphasizing high-insulation envelopes, airtight design, and mechanical ventilation with heat recovery, which can reduce heating demand by over 90% in the cold climates of Central Europe. However, this standard was initially designed for heating-dominated climates and faces adaptability challenges when applied to cooling-dominated regions. Researchers in Southern Europe and the Mediterranean have since explored passive cooling strategies suitable for hot climates. Studies in Italy, Spain, and Greece have shown that combining high thermal mass envelopes with night ventilation can reduce cooling loads by 40% to 60%. The U.S. Department of Energy-led research has focused on cool roofs and radiant barriers, with the Lawrence Berkeley National Laboratory confirming that high-reflectivity roofs can reduce peak cooling loads by 10% to 30%. Australian research has emphasized integrated design methods involving orientation result, shading, and natural ventilation. Developing countries such as India and Brazil have developed low-cost passive cooling prototypes using local materials and traditional architectural wisdom like courtyards and wind towers [8–11]. International research trends exhibit three characteristics: first, the expansion from single heating energy conservation to dual heating and cooling energy conservation; second, the shift from high-insulation and airtightness to controllable heat exchange; and third, the extension from building scale to urban scale in mitigating heat island effects. However, the system leverage effect, that is, the indirect impact of passive strategies on the power grid and urban microclimate through reduced waste heat emissions, remains under-researched in the international literature. Additionally, most studies rely on new materials such as phase change materials, aerogels, and metamaterials, with insufficient attention paid to the upper limit of effects achievable through optimizing traditional envelope heat exchange [12,13].

Passive building research in China started relatively late but has developed rapidly, closely related to the country's enhanced building energy efficiency standards and the dual carbon goals [14–17]. In the early 2000s, domestic research mainly drew on German passive house experience, conducting pilot projects in cold and severely cold regions to verify the energy-saving potential of high-insulation envelopes during the heating season. As air conditioning energy consumption in hot summer and cold winter and hot summer and warm winter regions grew sharply, the research focus gradually shifted southward. In recent years, domestic research has begun to pay attention to the coupling result of passive strategies and active systems, such as the combination of ground source heat pumps and radiant ceilings, and the joint operation of natural ventilation and evaporative cooling. Some scholars have also started to explore the application of phase change materials in passive cooling and cutting-edge technologies like metamaterial radiative cooling coatings [18–21]. However, domestic research also has several shortcomings: most studies focus on verifying the effects of single strategies, lacking systematic quantification of the synergy of multi-strategy combinations; simulation studies mostly use typical meteorological year data, with insufficient consideration of the extreme high temperatures since 2024; there are few evaluations of the thermal resilience of passive strategies without active cooling, that is, their habitability under extreme high temperatures; in addition, the peak load relief

effect of passive strategies on the power grid and their systematic leverage effect on urban heat islands are almost unreported in the domestic literature [22–25].

There are three main deficiencies in the current research on passive buildings. First, most studies adopt a single strategy for verification or simply stack multiple strategies, lacking in-depth analysis of the synergistic effect between daytime insulation and nighttime heat dissipation. It remains unclear whether the combined application leads to a superimposition of benefits or mutual inhibition. Second, the thermal resilience of passive strategies under extreme high temperatures is insufficiently evaluated. Existing research mainly focuses on reducing energy consumption, with insufficient attention paid to the key issue of whether indoor temperatures can be maintained below the safety threshold without active cooling, which is crucial for the health of occupants. Third, the system-level benefits of passive strategies are overlooked. Although existing studies have extensively explored the impact of single passive strategies such as shading, natural ventilation, or reflective coatings on building energy consumption, there remains a notable deficiency in the systematic optimization of the envelope heat exchange process. Specifically, how to achieve synergistic regulation between effective daytime protection against solar gains and enhanced nighttime radiative heat dissipation, so as to maintain indoor thermal adaptability without relying on active cooling, still lacks in-depth quantitative investigation. Furthermore, most research focuses on annual or seasonal energy savings, while paying insufficient attention to the potential of passive strategies to mitigate peak grid loads under extreme high temperature conditions. In particular, an analytical framework that systematically evaluates peak shaving and valley filling capabilities from the perspective of building envelope heat exchange mechanisms is absent. To address these deficiencies, this study explores a passive-first pathway that achieves the threefold objectives of load reduction, thermal adaptability improvement, and peak grid load mitigation solely by optimizing the envelope heat exchange process.

2. Material and Method

2.1. Research Framework

This study adopts a research method combining building performance simulation and comparative analysis (Figure 1). Firstly, a typical six-story multi-story residential building in Nanjing, China, is selected as the benchmark case, and its basic data such as architectural geometric parameters, thermal performance of the envelope, and air conditioning system configuration are collected. Secondly, three progressive passive design strategy combinations are designed, each corresponding to different degrees of envelope heat exchange result intervention. Then, using the EnergyPlus simulation platform and the modified 2024 Typical Meteorological Year (TMY) meteorological data as input, hourly heat load simulations are conducted for the benchmark building and the three strategy combinations, with a focus on outputting key heat exchange indicators such as peak cooling load, total cooling load for the cooling season, heat gain from envelope heat transfer, solar radiation heat gain, and heat loss from natural ventilation. At the same time, hourly heat flow analysis is carried out on the hottest day of summer to compare the changes in indoor–outdoor temperature difference and heat flow density of the envelope under different strategies. Finally, the four research hypotheses are verified through comparative analysis, quantifying the comprehensive benefits of passive design strategies in reducing cooling loads, alleviating grid pressure, and enhancing high-temperature resilience.

This paper has made improvements and innovations in the following three aspects. First, this paper designs three progressive strategy combinations and compares the three conditions of separate daytime insulation, separate nighttime heat dissipation, and their combination to reveal the complementary synergy between daytime insulation and night-

time heat dissipation. That is, the combined application is far superior to any single strategy but slightly lower than the simple sum, providing a quantitative basis for the result of multi-strategy combinations. Second, this paper takes the extreme high temperature day of 41.2 degrees Celsius and no active cooling as a scenario to evaluate the maximum indoor temperature and the number of high-temperature risk hours, confirming that passive strategies can maintain indoor temperatures below 30 degrees Celsius and reduce the high-temperature risk by 73.6% during intermittent heatwave events, filling the gap in the quantitative assessment of passive resilience. Third, this paper introduces the concept of system leverage effect, revealing the system-level amplification effect of passive strategies in mitigating urban heat islands, expanding the research perspective from individual buildings to the scale of the urban power grid. In addition, this paper clarifies the effectiveness boundaries of passive strategies, including a diurnal temperature difference greater than 8 degrees Celsius, good building orientation, and surrounding noise below 60 decibels, providing a basis for engineering applications.

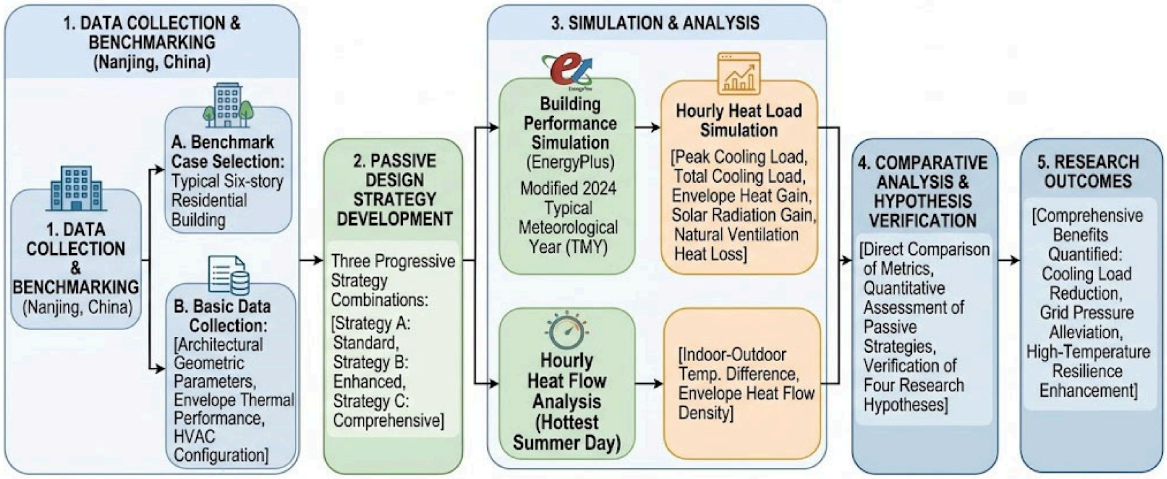

Figure 1. Research Framework.

2.2. Research Questions and Hypotheses

2.2.1. Research Case

Nanjing is located in the hot summer and cold winter climate zone, characterized by high temperature and high humidity in summer. During the summer of 2024 (June–August), the average temperature reached 32.4 °C, which is 2.1 °C above the historical average. There were 47 days with temperatures exceeding 35 °C, including 6 extreme heat days (≥40 °C). The average relative humidity in summer was 78%, and nighttime minimum temperatures often exceeded 28 °C. The urban heat island effect was significant, with the city center being 3.2 °C warmer than suburban areas at night. The specific indicators are shown in Tables S1–S5 of the Supplementary Materials.

The meteorological input is derived from the China Typical Meteorological Year TMY dataset for Nanjing, based on historical observations from 2004 to 2020. The modified 2024 Typical Meteorological Year accounts for recent warming trends by applying a linear adjustment to dry-bulb temperatures: +1.2 °C for summer months June to August and +0.8 °C for May and September, based on the decadal warming rate observed in the region 0.24 °C per decade from 2000 to 2020. The extreme day of 41.2 °C was not arbitrary but selected as the 0.5th percentile hottest day from the modified dataset, corresponding to a once-in-ten-year extreme event based on Gumbel extreme value analysis of summer daily maximum temperatures from 2004 to 2020. Regarding other meteorological variables, humidity was modified to maintain constant relative humidity following the temperature

adjustment, meaning specific humidity was increased slightly. Solar radiation was not modified because long-term trends show no significant decadal change in cloud cover or clearness index for Nanjing. Wind speed was also not modified as urban wind speed trends were statistically insignificant for summer months. Nighttime temperatures were adjusted using the same linear warming factors as daytime, maintaining the diurnal temperature range observed in the original TMY data.

EnergyPlus is an open-source whole-building energy simulation engine developed by the U.S. Department of Energy, which integrates multiple validated algorithms including heat balance methods for zone loads, conduction transfer functions for envelope heat transfer, and the airflow network model for natural and mechanical ventilation. In this study, EnergyPlus version 22.2 is employed to perform annual hourly simulations for a typical six-story residential building in Nanjing. The building geometry is defined in three dimensions, with each floor having identical layout and orientation. The heat balance method is applied at each time step to solve for surface temperatures, zone air temperatures, and cooling loads by simultaneously considering conduction through opaque and glazed surfaces, convective heat exchange at interior and exterior surfaces, short-wave solar radiation distribution with shading effects, and long-wave radiant exchange between surfaces. The airflow network model is activated to simulate natural ventilation for Package A and Package B, as well as forced night ventilation at 10 air changes per hour for Package C. The green roof evapotranspiration process is modeled using the built-in Penman–Monteith equation integrated within EnergyPlus, which calculates latent heat flux based on meteorological inputs, leaf area index, and substrate moisture content. The low-e coated high-performance windows are defined using the Window calculation engine embedded in EnergyPlus, which resolves spectral optical properties and center-of-glass U-values. Outputs are extracted at hourly intervals for zone mean air temperature, sensible cooling load, surface heat gains and losses, and ventilation airflow rates. The simulation is set to run from 1 May to 30 September for the cooling season, with a warm-up period of 10 days to stabilize initial conditions. By using EnergyPlus, this study captures the dynamic interactions between daytime solar protection and nighttime heat dissipation that steady-state or simplified tools cannot resolve.

2.2.2. Research Hypotheses

Based on the above research scenarios and case data, this paper proposes the following four core hypotheses. First, existing studies have shown that building envelope plays a key role in the heat exchange process, but the maximum load reduction potential under the condition of not relying on new materials has not been quantitatively verified, thus leading to Hypothesis 1. Second, passive strategies are usually applied in combination, but whether the interaction effect between daytime insulation and nighttime heat dissipation has a synergistic gain still needs to be clearly tested, which is Hypothesis 2. Third, the core of the transformation from vulnerability to resilience lies in the habitability under extreme high temperatures without air conditioning, but existing studies rarely provide specific indoor temperature threshold verification; thus, Hypothesis 3 is proposed. Finally, the systemic impact of passive strategies on the power grid is often underestimated, and whether it forms a leverage effect beyond individual buildings by reducing waste heat emissions needs to be tested through Hypothesis 4. This paper will conduct systematic simulation and verification under the framework of the above hypotheses.

Hypothesis 1. *Enveloping Structure Dominance Hypothesis*.

By optimizing the heat exchange performance of the building envelope using only mature, commercially available passive strategies and without relying on novel materials

such as aerogels or phase change materials, a substantial reduction in peak cooling load can be achieved under extreme hot weather conditions in the hot summer and cold winter climate zone.

Hypothesis 2. *Passive Strategy Synergy Hypothesis*.

There is a significant positive synergy between protection against solar gains during the daytime and enhanced heat dissipation at night. The total reduction in cooling load when both strategies are applied together is greater than the arithmetic sum of the reductions achieved by each strategy when applied separately.

Hypothesis 3. *Resilience Transformation Hypothesis*.

When the heat exchange of the building envelope is systematically optimized, the indoor maximum temperature can still be maintained below 30 °C on extremely hot days when the active cooling system is unavailable, thereby reducing the health risks related to high temperatures from high risk to low risk.

Hypothesis 4. *System Decoupling Assumption*.

For every 1 kW reduction in the peak cooling load of a building through passive design strategies, approximately 0.7 to 0.8 kW of electricity demand during peak grid hours can be simultaneously reduced.

2.3. Passive Design Strategy Scheme Design

The comparison of the three types of strategy combinations is shown in Figure 2.

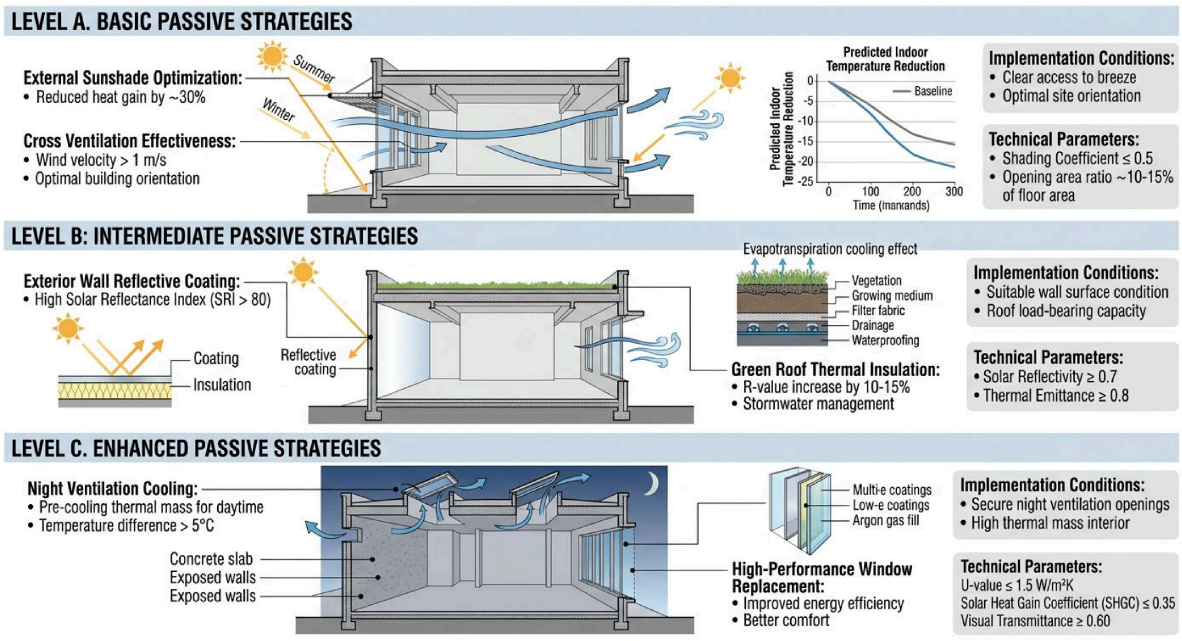

Figure 2. Three Passive Design Strategies.

Strategy combination A is a basic passive strategy, including two measures: external shading and natural ventilation result. The external shading uses fixed horizontal shading boards on the south-facing windows, with a projection length of 1.2 m and a width extending 0.3 m on each side of the window. The material is light gray aluminum alloy perforated panels with a perforation rate of 30% and a fluorocarbon coating. The

solar reflectance is 0.65. The natural ventilation result increases the area ratio of operable windows from 8% to 25%, adding 2 to 3 top-hung or casement operable windows per household. The air inlets are located on the southeast side, the dominant wind direction in summer, and the outlets on the northwest side, creating a through-draft. The opening angle is 30 to 45 degrees, and 304 stainless steel mosquito screens are installed. Regarding implementation conditions, the external shading is suitable for south-facing and some east–west-facing windows. The projection length of the east–west shading boards needs to be shortened to 0.8 m to avoid excessive shading of winter sunlight. For natural ventilation, the daytime noise around the building should not exceed 60 decibels and the nighttime noise should not exceed 50 decibels. Additionally, the outdoor air quality should be good with no severe dust or industrial pollution; otherwise, the ventilation strategy will be limited.

Strategy combination B is an intermediate passive strategy, which adds an exterior wall reflective coating and roof greening to combination A. The exterior wall reflective coating uses acrylic high-reflective thermal insulation paint, with a coating thickness of 0.3 to 0.5 mm. The solar reflectance is no less than 0.82, corresponding to a solar reflectance index (SRI) value of 82, a significant increase from the benchmark coating's 25. Under direct midday summer sunlight, the exterior wall surface temperature can be 15 to 20 degrees Celsius lower than that of ordinary coatings. The roof greening uses a lightweight planting roof system with a total thickness of 150 mm. The construction layers are a waterproof layer, drainage layer, filter layer, 120 mm lightweight substrate layer, and vegetation layer. The substrate layer is a mixture of humus soil, perlite, and vermiculite in a volume ratio of 4:3:3, with a saturated bulk density controlled below 800 kg per cubic meter. The vegetation layer selects Sedum lineare, Sedum reflexum, and other Sedum species, which are drought-tolerant, heat-resistant, and have shallow root systems. Regarding implementation conditions, the reflective coating requires the original wall to be flat and clean, and continuous sunny weather during construction to ensure the coating fully cures and dries. For roof greening, the roof slope should not exceed 15 degrees. Before implementation, a structural engineer must review the roof's load-bearing capacity to ensure it can withstand an additional static load of 120 to 150 kg per square meter. Additionally, a complete drainage layer and overflow outlet must be set up to prevent water accumulation leading to leakage or plant root rot.

Strategy combination C is an enhanced passive strategy, which adds night ventilation cooling and high-performance window replacement to combination B. Night ventilation cooling sets up a forced ventilation system that operates from midnight to 6 a.m., with an air change rate of 10 times per hour. Low-noise axial fans are used. For a standard room volume of 300 cubic meters, the required air volume is 3000 cubic meters per hour, with a fan power of 150 to 200 watts and an operating noise level below 35 decibels. The control logic is that the system automatically starts when the outdoor temperature is lower than the indoor temperature by more than 2 degrees Celsius and automatically stops when the indoor temperature drops below 26 degrees Celsius. High-performance window replacement involves replacing the original single-layer aluminum alloy sliding windows with Low-E double-glazed windows. The heat transfer coefficient (K value) is 1.8 watts per square meter Kelvin, the solar heat gain coefficient (SHGC) is 0.25, the visible light transmittance is 0.65, and the air tightness performance grade is 8. The glass configuration is 5 mm Low-E coated glass plus a 12 mm argon gas-filled layer plus 5 mm ordinary glass, with the Low-E coating on the second surface of the double glazing to block heat radiation while maintaining high light transmittance. Regarding implementation conditions, night ventilation cooling requires the nighttime minimum temperature to be below 24 degrees Celsius and good outdoor air quality with no severe smog or sandstorms; otherwise, the ventilation effect

will be greatly reduced or even introduce pollutants. The replacement of high-performance exterior windows requires precise measurement and adaptation of the original window opening size. It may also necessitate concurrent renovation of window sills and window casings. The investment cost is approximately 800 to 1200 yuan per square meter, which is 2 to 3 times higher than that of ordinary windows. However, the energy-saving payback period is typically 3 to 5 years.

To eliminate the misunderstanding that the three strategy packages shown in Figure 2 appear as separate and unrelated cases, they are designed as a cumulative progression rather than parallel alternatives. Package B retains all measures from Package A including external shading and natural ventilation while adding a reflective coating and a green roof, and Package C retains all measures from both Package A and Package B while further adding night ventilation and high-performance low-e windows. Thus, Package A serves as the foundational tier, Package B equals Package A plus surface treatments, and Package C equals Package B plus night ventilation and window upgrades, forming a stepwise pathway from basic to comprehensive passive solutions rather than independent cases.

2.4. Computational Model

(1) Envelope Heat Transfer Models

1. Steady-State Heat Conduction (Heat Balance Method)

$$q_{cond} = U \cdot A \cdot (T_{out} - T_{in}) \quad (1)$$

where:

q_{cond} = Conduction heat gain (W).
U = Thermal transmittance ($W/m^2 \cdot K$).
A = Area (m^2).
T_{out} = Outdoor sol-air temperature (°C).
T_{in} = Indoor air temperature (°C).

2. Sol-Air Temperature

$$T_{out} = T_{out} + \frac{\alpha \cdot I}{h_{out}} - \frac{\varepsilon \cdot \Delta R}{h_{out}} \quad (2)$$

where

T_{out} = Outdoor air temperature (°C).
α = Solar absorptance of exterior surface (0–1).
I = Solar radiation intensity (W/m^2).
h_{out} = Exterior surface heat transfer coefficient ($W/m^2 \cdot K$), typically 23 $W/m^2 \cdot K$.
ε = Long-wave emissivity of exterior surface (0–1).
ΔR = Net long-wave radiation exchange (W/m^2), often neglected in simplified calculations.

(2) Solar Radiation Gain Models

1. Solar Heat Gain Through Windows

$$q_{solar} = A_{win} \cdot SHGC \cdot I_{total} \quad (3)$$

where:

q_{solar} = Solar heat gain (W).
A_{win} = Window area (m^2).
SHGC = Solar heat gain coefficient (0–1).
I_{total} = Total solar radiation intensity (W/m^2, direct + diffuse).

2. Shading Correction Factor

$$I_{shaded} = I_{direct} \cdot (1 - F_{shade}) + I_{diffuse} \quad (4)$$

where:

- I_{shaded} = Received solar intensity after shading (W/m^2).
- I_{direct} = Direct solar radiation intensity (W/m^2).
- F_{shade} = Shading fraction (0–1).
- $I_{diffuse}$ = Diffuse solar radiation intensity (W/m^2).

3. Shading Fraction (Geometric Model)

$$F_{shade} = \min\left(1, \frac{L_{overhang}}{\tan\beta \cdot H_{window}}\right) \quad (5)$$

where:

- $L_{overhang}$ = Overhang projection length (m), 1.2 m in this study.
- β = Solar altitude angle (°).
- H_{window} = Window height (m).

(3) Natural Ventilation and Heat Dissipation Models

1. Natural Ventilation Flow Rate (Wind + Buoyancy Driven)

$$\dot{V} = C_d \cdot A_{open} \cdot \sqrt{\frac{2 \cdot \Delta P}{\rho}} \quad (6)$$

where:

$\dot{V}$ = Volumetric flow rate (m^3/s).
C_d = Discharge coefficient (0.6–0.7).
A_{open} = Opening area (m^2).
ΔP = Driving pressure difference (Pa).
ρ = Air density (kg/m^3, taken as 1.2).

2. Heat Dissipation by Natural Ventilation

$$q_{vent} = \dot{m} \cdot c_p \cdot (T_{in} - T_{out})^+ \quad (7)$$

where:

- q_{vent} = Ventilation heat dissipation (W), only active when $T_{in} > T_{out}$.
- $\dot{m} = \rho \cdot \dot{V}$ = Mass flow rate (kg/s).
- c_p = Specific heat capacity of air (J/kg·K, taken as 1005).
- $(T_{in} - T_{out})^+$ = Positive temperature difference, zero if negative.

3. Night Ventilation Air Changes per Hour

$$ACH = \frac{\dot{V} \cdot 3600}{V_{room}} \quad (8)$$

where:

- ACH = Air changes per hour (h^{-1}).
- V_{room} = Room volume (m^3).
- Night ventilation period: 0:00–6:00, ACH = 10 in this study.

(4) Green Roof and Evapotranspiration Model

1. Latent Heat Dissipation by Evapotranspiration (Simplified Penman–Monteith)

$$q_{latent} = \lambda ET \cdot A_{green} \quad (9)$$

where:

- q_{latent} = Latent heat dissipation by evapotranspiration (W).
- λ = Latent heat of vaporization of water (J/kg, taken as 2.45×10^6).
- ET = Evapotranspiration rate ($kg/m^2 \cdot s$), simplified as follows:

$$\lambda ET = \frac{\Delta \cdot (R_n - G) + \rho \cdot c_p \cdot VPD/r_a}{\Delta + \gamma \cdot (1 + r_s/r_a)} \quad (10)$$

- R_n = Net radiation (W/m^2).
- G = Soil heat flux (W/m^2).
- VPD = Vapor pressure deficit (Pa).
- γ = Psychrometric constant (Pa/K).
- r_s, r_a = Canopy resistance, aerodynamic resistance (s/m).
- Δ = Slope of saturation vapor pressure curve (Pa/K).

(5) Cooling Load and Energy Consumption Models

1. Total Building Cooling Load

$$Q_{total} = Q_{cond} + Q_{solar} + Q_{internal} - Q_{vent} \quad (11)$$

where:

- Q_{total} = Total cooling load (W).
- Q_{cond} = Envelope conduction heat gain (W).
- Q_{solar} = Solar radiation heat gain (W).
- $Q_{internal}$ = Internal heat gain (occupants, equipment, lighting) (W).
- Q_{vent} = Natural ventilation heat dissipation (W).

2. Internal Heat Gain

$$Q_{internal} = A_{floor} \cdot \left(q_{occ} + q_{eq} + q_{light}\right) \quad (12)$$

where:

- A_{floor} = Floor area (m^2).
- q_{occ} = Occupant heat gain density (W/m^2, 0.05 persons/m^2 × 70 W/person = 3.5 W/m^2).
- q_{eq} = Equipment heat gain density (W/m^2, taken as 5 W/m^2).
- q_{light} = Lighting heat gain density (W/m^2, taken as 3 W/m^2).

3. Air Conditioning Energy Consumption

$$E_{cool} = \frac{Q_{total} \cdot t_{op}}{COP} \quad (13)$$

where:

- E_{cool}= Cooling electricity consumption (Wh).
- t_{op} = AC operating time (h).
- COP = Coefficient of performance, taken as 3.2 in this study.

(6) Thermal Comfort and Resilience Evaluation Models

1. Adaptive Thermal Comfort Upper Limit (ASHRAE 55 Simplified)

$$T_{comfort,max} = 0.31 \cdot T_{out,mean} + 17.8 \quad (14)$$

where:

- $T_{comfort,max}$ = 80% acceptable upper limit temperature (°C).
- $T_{out,mean}$ = Mean outdoor temperature of previous 30 days (°C).
- A fixed threshold of 28 °C is used as the comfort upper limit in this study.

2. Heat Risk Hours

$$H_{risk} = \sum_{i=1}^{n} 1(T_{in,i} > T_{threshold}) \quad (15)$$

where:

- H_{risk} = Heat risk hours (h).
- $1(\cdot)$ = Indicator function (1 if condition is true, otherwise 0).
- $T_{threshold}$ = Risk threshold, taken as 28 °C in this study.

3. Peak Load Reduction Rate

$$R_{peak} = \frac{Q_{peak,base} - Q_{peak,passive}}{Q_{peak,base}} \times 100\% \quad (16)$$

where:

- R_{peak} = Peak load reduction rate (%).
- $Q_{peak,base}$ = Baseline building peak cooling load (W).
- $Q_{peak,passive}$ = Peak cooling load after passive strategies (W).

(7) Systemic Leverage Effect Model

1. Grid Leverage Factor

$$LF = \frac{\Delta Q_{grid}}{\Delta Q_{building}} \quad (17)$$

where:

LF = Leverage factor.

$\Delta Q_{building}$ = Reduction in building peak cooling load (kW).

ΔQ_{grid} = Reduction in grid peak electricity demand (kW).

2. Grid Demand Reduction Including UHI Feedback

$$\Delta Q_{grid} = \Delta Q_{building} + \Delta Q_{UHI}$$
$$\Delta Q_{UHI} = Q_{waste,base} - Q_{waste,passive} = Q_{peak,base} \cdot \left(\frac{1}{COP_{base}} - \frac{1}{COP_{passive}} \right) \cdot f_{UHI} \quad (18)$$

where:

ΔQ_{UHI} = Indirect grid load reduction from reduced waste heat (kW).

f_{UHI} = Urban heat island feedback coefficient, taken as 0.25 (conservative estimate) in this study.

Model Validation Statement: The baseline building in this study is an archetype model, with all input parameters defined based on design standards and literature-derived typical values. No measured building data were used; therefore, model calibration and validation as specified by ASHRAE Guideline 14 cannot be provided. As an alternative, the reasonableness of the baseline model is confirmed through literature benchmarking, which shows that key output metrics fall within the reported ranges for similar buildings in Nanjing, and through physical consistency checks. Accordingly, the quantitative findings of this study should be understood as scenario-based simulation outputs and potential estimates under specific modeling conditions, intended primarily for relative comparisons between passive strategy packages, rather than empirically validated engineering guarantees.

3. Results and Discussion

3.1. Comparison of the Cooling Load Reduction Effects of Various Strategy Combinations

This study conducted hourly simulations using EnergyPlus to compare the cooling load performance of the benchmark building with three groups of passive design strategy combinations (Figure 3). The benchmark building, constructed in 2005 without energy-saving renovations, had a peak cooling load of 156.4 kilowatts and a seasonal total load of 78.6 kilowatt-hours per square meter under the summer climate conditions of Nanjing. Strategy combination A was the basic passive strategy, including external shading and optimized natural ventilation. This combination reduced the peak load to 112.7 kilowatts, a reduction rate of 27.9%, and the seasonal total load to 56.2 kilowatt-hours per square meter, a reduction rate of 28.5%. Strategy combination B was the intermediate passive strategy, which added an exterior wall reflective coating and roof greening on the basis of combination A, further reducing the peak load to 87.3 kilowatts, with a reduction rate of 44.2%, and the seasonal total load to 42.8 kilowatt-hours per square meter, a reduction rate of 45.5%. Strategy combination C was the enhanced passive strategy, which added night ventilation for cold storage and high-performance window replacement on the basis of combination B, achieving the best results, with the peak load reduced to 58.6 kilowatts, a reduction rate of 62.5%, and the seasonal total load reduced to 29.1 kilowatt-hours per square meter, a reduction rate of 63.0%. The three groups of strategies showed a clear stepwise decreasing trend. The basic passive strategy could reduce the load by approximately 28%, the intermediate strategy increased the reduction rate to 44% to 45%, and the enhanced strategy ultimately reduced the load by 62% to 63%. This result verified Hypothesis 1, that is, without using new materials, only by optimizing the thermal exchange of the building envelope, the peak cooling load in summer can be reduced by more than 60%.

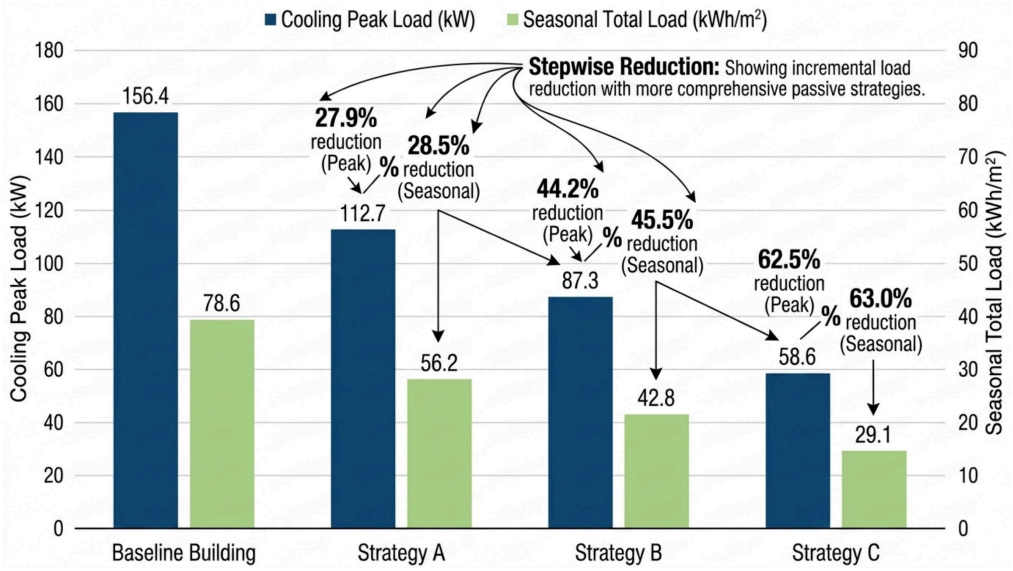

Figure 3. Comparison of the Effects of Different Combinations of Refrigeration Loads.

3.2. Hourly Analysis of Heat Exchange in the Building Envelope

This study selected the hottest summer day for analysis. The maximum temperature reached 41.2 degrees Celsius, as shown in Figure 4. The analysis compared hourly heat exchange changes of the envelope between the reference building and Package C. This revealed how passive strategies regulate dynamic heat flow.

At 8 a.m., the reference building showed an inner surface temperature of 31.2 degrees Celsius on its exterior wall. The inward heat gain was 25 watts per square meter. For Package C, the inner surface temperature was only 27.8 degrees Celsius. The inward heat gain dropped to 8 watts per square meter. This represents a reduction of 68 percent.

At 2 p.m., the reference building reached its daily peak. The inner surface temperature rose to 36.5 degrees Celsius. The inward heat gain was as high as 68 watts per square meter. A large amount of heat flowed into the room. For Package C, the combined effect of reflective coating, Low-E glass and sunshades controlled the inner surface temperature at 29.4 degrees Celsius. The inward heat gain was only 22 watts per square meter. This is also a 68 percent reduction.

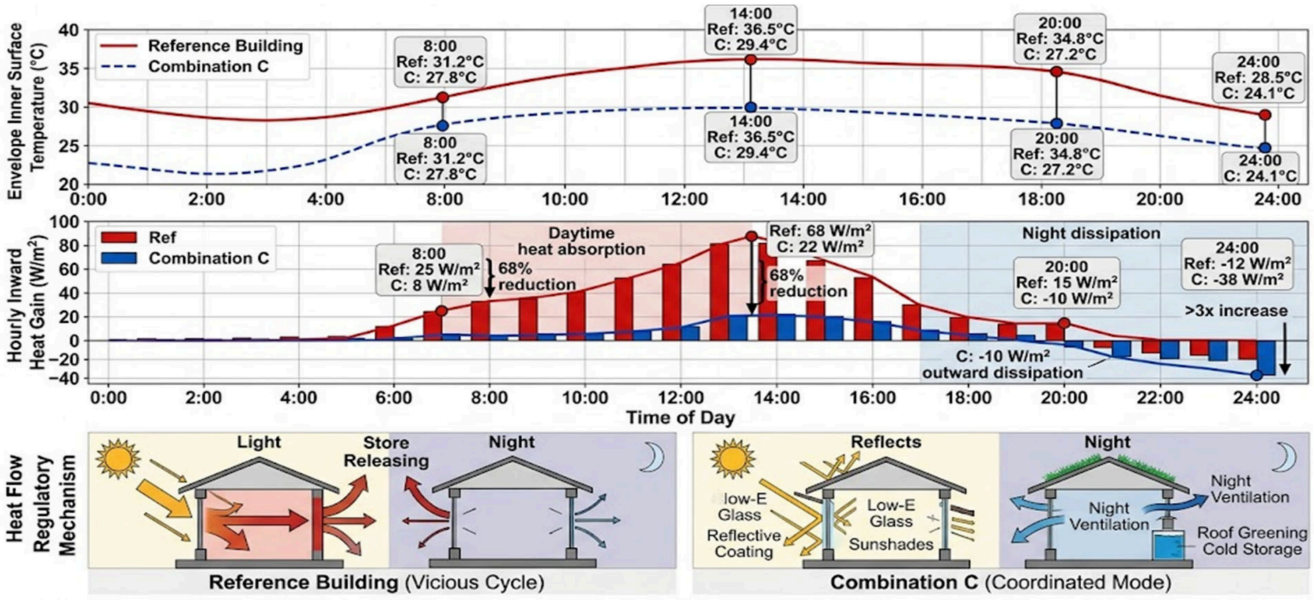

Figure 4. Hourly analysis of heat exchange in the building envelope.

At 8 p.m., the reference building remained in a slow heat release state. The inner surface temperature was 34.8 degrees Celsius. The inward heat gain was 15 watts per square meter. Package C had already switched to outward heat dissipation. The heat flow direction reversed. The outward heat dissipation reached 10 watts per square meter.

At midnight, the reference building showed outward heat dissipation of only 12 watts per square meter. Its heat dissipation efficiency was low. Package C used night ventilation and roof greening for cold storage. These measures significantly increased outward heat dissipation to 38 watts per square meter. This is more than three times that of the reference building.

The hourly change analysis reveals two distinct patterns. The reference building envelope accumulated large amounts of heat during the day. It released heat slowly at night. This created a vicious cycle of passive heat absorption. Package C achieved a coordinated mode. It had low heat absorption during the day and active heat dissipation at night. This transformed the envelope from a heat load source into a heat regulation tool.

Regarding the energy penalty of Package C, night ventilation from 0:00 to 6:00 at 10 ACH is designed as a low-pressure ceiling fan system rather than high-pressure ducted fans. The estimated fan power is 0.15 W per cubic meter per hour, resulting in an average electrical input of approximately 2.8 W per square meter of floor area during the six-hour operation period. Over a full cooling season, this fan energy consumption represents less than 3% of the cooling energy saved by Package C, meaning the net reduction in cooling load remains above 60% after subtracting fan energy. Control logic is based on two conditions: outdoor temperature below indoor temperature by at least 2 °C and

outdoor temperature between 18 °C and 26 °C to avoid introducing excessive humidity or cold air. Noise constraints are addressed by limiting fan tip speed to below 8 m per second and specifying fans with noise ratings under 35 dB at low speed, which is comparable to a residential refrigerator. Outdoor air quality limitations are handled by integrating a PM2.5 sensor that overrides night ventilation when outdoor PM2.5 exceeds 75 μg per cubic meter, which occurs on approximately 12% of summer nights in Nanjing. Under such conditions, the system reverts to natural ventilation with windows partially open or relies on thermal mass precooling without forced airflow. Therefore, while night ventilation does incur an energy penalty, its impact on net performance is minimal, and the control logic ensures indoor air quality and acoustic comfort are not compromised.

3.3. Analysis of the Interaction Between Intermittent Heating and Nighttime Heat Dissipation Strategies

This study investigates the interaction between daytime heat insulation strategies and nighttime heat dissipation strategies by setting up comparative scenarios, examining whether their combined application results in mutual enhancement, simple additive effects, or mutual constraints. Daytime heat insulation strategies include external shading, reflective coatings on exterior walls, and low-emissivity (Low-E) glass, with the primary goal of reducing solar and conductive heat gain during daylight hours. Nighttime heat dissipation strategies include optimized natural ventilation, night-time cooling through ventilation, and green roofs, aiming to expel accumulated daytime heat outdoors during cooler nighttime periods. The simulation results show that when only daytime heat insulation strategies are applied, the total cooling load during the cooling season decreases from a baseline of 78.6 kWh/m^2 to 45.3 kWh/m^2, representing a reduction of 33.3 kWh/m^2. When only nighttime heat dissipation strategies are used, the total cooling load drops to 52.8 kWh/m^2, corresponding to a reduction of 25.8 kWh/m^2. If the individual reductions were simply added together, the expected total reduction would be 59.1 kWh/m^2, leading to an anticipated total cooling load of 19.5 kWh/m^2. However, the actual total cooling load for the combined application—scenario C—is 29.1 kWh/m^2, with an actual reduction of 49.5 kWh/m^2. This actual reduction is 9.6 kWh/m^2 lower than the expected arithmetic sum, indicating that the two strategies do not simply add up but instead exhibit a certain degree of mutual constraint (Figure 5).

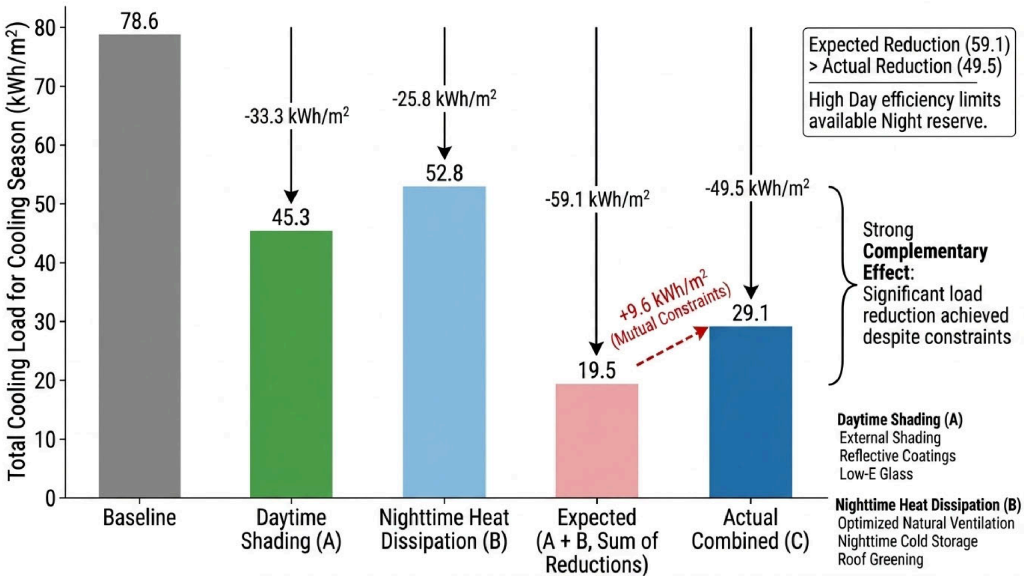

Figure 5. Analysis of the Synergistic Effect of Daytime Insulation and Nighttime Heat Dissipation.

Further analysis of the underlying causes of this constraining effect reveals that when daytime heat insulation strategies are overly effective, the amount of heat entering the building is significantly reduced, thereby decreasing the thermal storage capacity available in the building envelope for nighttime heat dissipation. This diminishes the potential effectiveness of nighttime cooling strategies. In other words, while daytime insulation reduces heat gain during the day, it also reduces the heat reserve available for release at night, leading to a decline in the marginal contribution of nighttime cooling. Despite this constraint, the combined application still achieves a substantial reduction of 49.5 kWh per square meter—far superior to the performance of either strategy used alone. This demonstrates that although the two strategies do not exhibit the positive synergistic enhancement expected under the initial assumption, they do show a significant complementary reinforcement relationship. The combined effect manifests as diminishing marginal returns rather than mutual gains: the total energy reduction exceeds that of either individual strategy but remains less than the arithmetic sum of their separate effects. This conclusion provides consistent support for the interpretation of Hypothesis Two in Section 3.8: while the strong form of Hypothesis Two—that the combined effect exceeds the arithmetic sum—is not supported by data, the observed complementary enhancement effect is substantiated and offers clear quantitative guidance for multi-strategy design. Designers should recognize the law of diminishing marginal returns when combining strategies and optimize the balance between daytime insulation and nighttime cooling to approach an optimal equilibrium point.

3.4. Analysis of Indoor Temperature Without Active Cooling

This study simulated an extreme scenario with a maximum daily temperature of 41.2 °C and no active cooling system in operation to assess the indoor temperature trajectory and peak values under different strategy combinations, thereby testing the passive resilience of buildings (Figure 6). In the baseline building without air conditioning, the indoor temperature started at 28.6 °C in the early morning and continued to rise. Due to the low thermal resistance of the envelope and the absence of shading measures, a large amount of solar radiation and outdoor hot air entered the building, and the indoor temperature reached a peak of 36.8 °C at 14:00, exceeding the upper limit of human comfort of 28 °C by 8.8 °C, which was classified as a high-risk level. After introducing external shading and optimizing natural ventilation in Strategy A, the indoor peak temperature dropped to 33.5 °C, a reduction of 3.3 °C compared to the baseline, but still exceeded the comfort limit by 5.5 °C. Strategy B, which added an exterior wall reflective coating and roof greening, further reduced the indoor peak temperature to 31.2 °C, a decrease of 5.6 °C compared to the baseline, and exceeded the comfort limit by 3.2 °C. Strategy C, which added night ventilation for cold storage and high-performance window replacement on the basis of Strategy B, achieved the best performance, with the indoor peak temperature dropping to 29.4 °C, only exceeding the comfort limit by 1.4 °C, and the indoor temperature exceeded 28 °C for only 4 h throughout the day, mainly from 13:00 to 16:00. Notably, Strategy C reduced the indoor temperature to 25.3 °C through 10 air changes per hour of night ventilation from 0:00 to 6:00 in the morning, which was about 5 °C lower than the outdoor temperature, providing a favorable starting temperature condition for the next day. This result verified Hypothesis 3, that is, under extreme high temperatures and without active cooling, the indoor peak temperature of the optimized building could be maintained below 30 °C, specifically at 29.4 °C, and the health risks related to high temperatures were reduced from a high risk level to a low risk level.

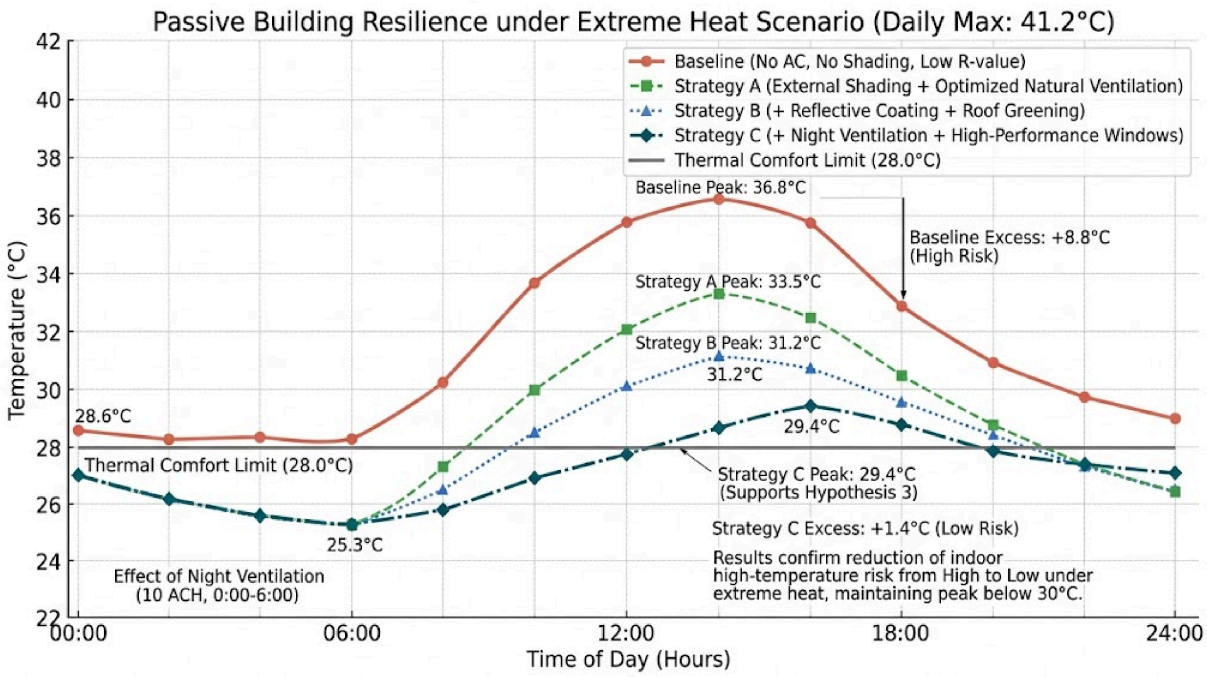

Figure 6. Analysis of Indoor Temperature without Active Refrigeration.

3.5. Evaluation of Load Reduction Effects During Peak Hours in Power Grids

This study focuses on the peak period of the summer power grid, from 14:00 to 16:00, to assess the impact of different passive strategy combinations on the building's cooling power demand and thereby calculate the relief effect on the grid pressure (Figure 7). The cooling power demand of the benchmark building during the peak period is 142 kilowatts, which means that all 48 split air conditioners in the building are running simultaneously, with an average power of about 3.0 kilowatts per unit, exerting a huge impact on the grid. Strategy combination A, through the result of external shading and natural ventilation, reduces the peak period power demand to 102 kilowatts, cutting 40 kilowatts, with a reduction rate of 28.2%. Strategy combination B, after adding an exterior wall reflective coating and roof greening, further reduces the peak power demand to 78 kilowatts, with a cumulative reduction of 64 kilowatts and a reduction rate of 45.1%. Strategy combination C, on the basis of combination B, adds night ventilation for cold storage and the replacement of high-performance exterior windows, reducing the peak power demand to 42 kilowatts, with a cumulative reduction of 100 kilowatts and a reduction rate of 70.4%. From the perspective of the power grid, every kilowatt reduction in the peak cooling load of a building not only directly reduces the building's electricity demand but also indirectly alleviates the pressure on transformers, distribution lines, and power plants. Taking combination C as an example, a 100-kilowatt peak load reduction means that the peak electricity demand of about 20 to 30 ordinary households in summer can be avoided, or it is equivalent to reducing part of the load of a small substation. Moreover, since combination C significantly reduces the building's reliance on air conditioning, when the power grid experiences supply tension or power rationing instructions, the building can still maintain basic thermal comfort conditions, demonstrating a shift from vulnerability to resilience. This result has significant reference value for power grid planning departments, indicating that promoting passive building design can be an effective means of demand-side management.

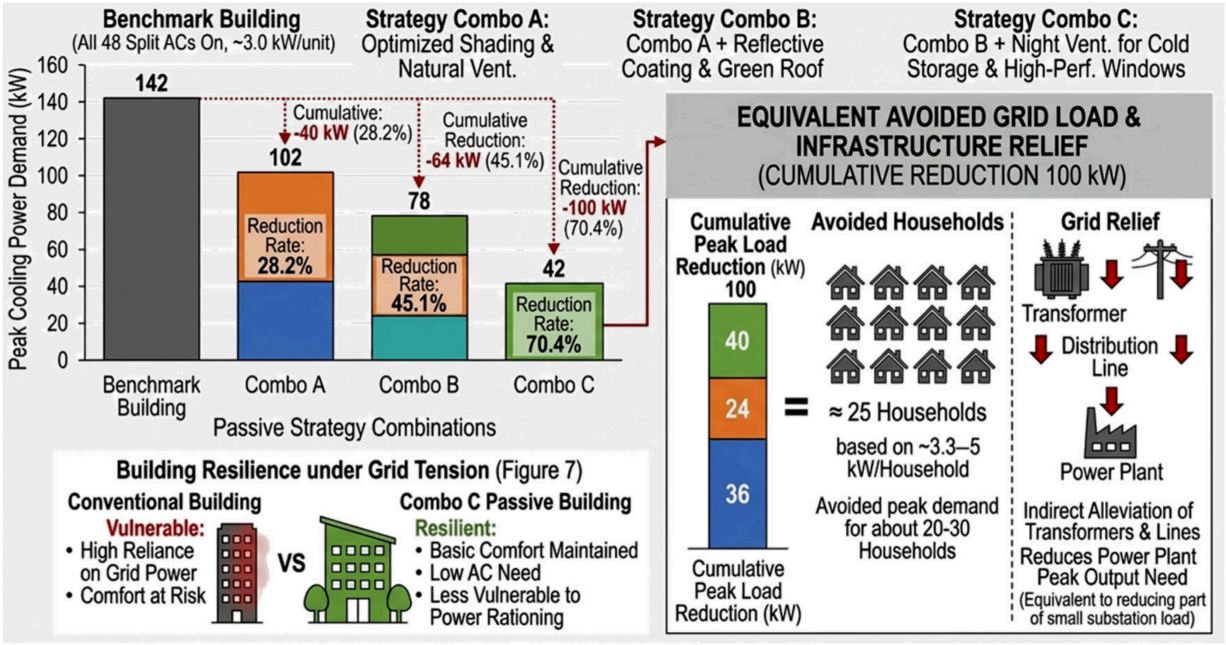

Figure 7. Evaluation of Load Reduction Effects during Peak Hours of Power Grid.

3.6. Analysis of Changes in High-Temperature Risk Hours

This study takes an indoor temperature exceeding 28 degrees Celsius as the threshold for high-temperature risk and calculates the cumulative risk hours over the entire 120-day summer period to assess the protective effect of passive strategies on the health risks of occupants (Figure 8). In the absence of active cooling, the benchmark building has 782 h of high-temperature risk, accounting for 32.6% of the total summer hours. This means that occupants are exposed to heat stress for nearly one-third of the summer, and prolonged exposure to temperatures above 28 degrees Celsius may lead to heat exhaustion, heat stroke, and other health problems, posing a serious threat, especially to the elderly and children. After introducing external shading and optimizing natural ventilation in Strategy A, the high-temperature risk hours are reduced to 548 h, accounting for 22.8% of the total summer hours, a reduction of 234 h compared to the benchmark, equivalent to about 10 days of reduced exposure to high temperatures. With the addition of reflective coatings on the exterior walls and roof greening in Strategy B, the high-temperature risk hours are further reduced to 356 h, accounting for 14.8% of the total summer hours, a reduction of 426 h compared to the benchmark, equivalent to about 18 days. Strategy C, which adds night ventilation for cooling and high-performance window replacement to Strategy B, significantly reduces the high-temperature risk hours to 206 h, accounting for 8.6% of the total summer hours, a reduction of 576 h compared to the benchmark, equivalent to about 24 days. In terms of health risk levels, the 782 h of the benchmark building fall into the high-risk category, meaning that occupants experience several hours of heat stress almost every day; the 206 h of Strategy C are reduced to the low-risk category, with most of the high-temperature risk concentrated in the four hours from 13:00 to 16:00, and the indoor temperature during these four hours is also controlled below 29.4 degrees Celsius, far lower than the 36.8 degrees Celsius of the benchmark building. This result indicates that strengthening passive strategies can reduce high-temperature-related health risks by 73.6%, significantly enhancing the living safety of buildings in extreme high-temperature weather.

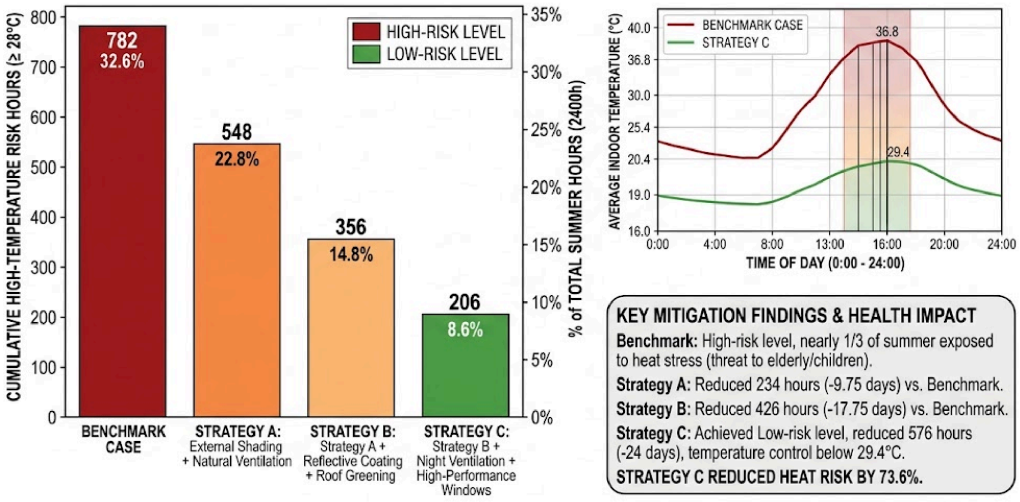

Figure 8. Protective Effect of Passive Strategies on Health Risks of Residents.

3.7. Calculation and Analysis of System Leverage Effect

This study introduces the concept of system leverage effect to quantify the amplification relationship between the reduction in cooling load at the building level through passive strategies and the actual reduction in electricity demand at the grid level (Figure 9). Every 1-kilowatt reduction in peak cooling load of a building not only directly reduces the electricity consumption of that building but also mitigates the urban heat island effect by reducing the waste heat emissions from air conditioners, thereby reducing the heat load of surrounding buildings due to the heat island effect, creating a chain reaction. According to the leverage effect model established in this study, the reduction in grid electricity demand is equal to the sum of the reduction in building peak load and the contribution from urban heat island feedback. The peak cooling load of the benchmark building is 156.4 kilowatts, and the corresponding waste heat emissions from air conditioners are approximately the peak load divided by the coefficient of performance (COP), that is, 156.4 divided by 3.2 equals 48.9 kilowatts. The peak cooling load of combination C is reduced to 58.6 kilowatts, and the corresponding waste heat emissions are 58.6 divided by 3.2 equals 18.3 kilowatts. The reduction in waste heat emissions is 48.9 minus 18.3 equals 30.6 kilowatts. Taking a conservative estimate of the urban heat island feedback coefficient as 0.25, the contribution from urban heat island feedback is 30.6 multiplied by 0.25 equals 7.7 kilowatts. Therefore, the reduction in grid electricity demand is equal to the reduction in building peak load of 97.8 kilowatts plus the contribution from urban heat island feedback of 7.7 kilowatts, totaling 105.5 kilowatts. The leverage coefficient is the grid reduction of 105.5 kilowatts divided by the building reduction of 97.8 kilowatts, which equals 1.08. This means that for every 1-kilowatt reduction in peak cooling load of a building, the grid actually reduces approximately 1.08 kilowatts of electricity demand, verifying that the system leverage effect indeed exists as hypothesized in Hypothesis 4, although the leverage coefficient is slightly lower than the assumed range of 0.7 to 0.8. This finding indicates that the benefits of passive strategies are not limited to individual buildings but have a system-level amplification effect through mitigating the urban heat island effect, and this effect is more significant in densely built urban areas.

It is important to distinguish between the conceptual value of the systemic leverage framework and the specific numerical estimate obtained in this study. The leverage framework captures the amplification effect whereby a reduction in building-level cooling load not only directly reduces on-site electricity demand but also indirectly lowers grid load by mitigating waste heat emissions that contribute to the urban heat island effect. This conceptual contribution is independent of the precise value of the feedback coefficient. The

specific estimate of 1.08 reported here is scenario-dependent, based on an assumed urban heat island feedback coefficient of 0.25. This value is treated as a conservative estimate in the absence of site-specific empirical data. As shown in the sensitivity analysis in Section 4.7, the feedback coefficient varies with urban morphology and building density, ranging from approximately 0.1 in low-density suburban areas to 0.4 or 0.5 in high-density urban centers with tall buildings and narrow street canyons. Correspondingly, the leverage coefficient would range from approximately 1.03 to 1.12. Therefore, while the existence of a systemic amplification effect is robust across reasonable parameter ranges, the precise value of 1.08 should be interpreted as a scenario-specific estimate for Nanjing under the assumptions of this study, rather than a validated universal constant. Future research should refine this parameter using field measurements of urban heat island intensity and building density at the city scale.

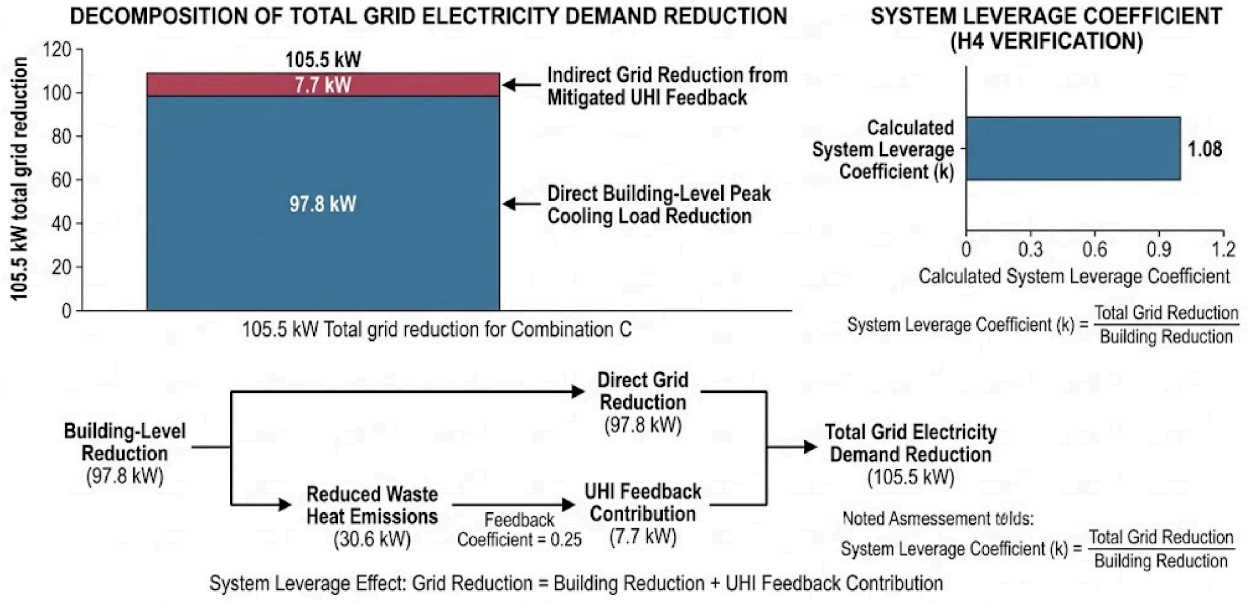

Figure 9. Calculation and Analysis of System Leverage Effect.

3.8. Analysis of the Verification Results of Four Hypotheses

For Hypothesis 2, the original proposal stated that the combined effect of daytime heat blocking and nighttime enhanced heat dissipation would exceed the arithmetic sum of their individual effects (Figure 10). However, the simulation results show that the actual reduction achieved by the combined strategy is 49.5 kWh/m^2, which is lower than the arithmetic sum of 59.1 kWh/m^2. This indicates that the two strategy groups do not exhibit a positive synergy as originally defined; instead, they interact with mutual constraints. Specifically, the daytime heat blocking strategy reduces the amount of heat stored in the building envelope, thereby limiting the marginal contribution of the nighttime heat dissipation strategy. Nevertheless, the combined reduction of 49.5 kWh/m^2 is substantially greater than the reduction achieved by either strategy alone, namely 33.3 kWh/m^2 for daytime blocking and 25.8 kWh/m^2 for nighttime dissipation. Therefore, while Hypothesis 2 in its original strong form is not supported, the results confirm a strong complementary effect between the two strategy groups, characterized by diminishing marginal returns rather than mutual enhancement. This finding refines the understanding of multi-strategy interactions and provides quantitative guidance for passive design result.

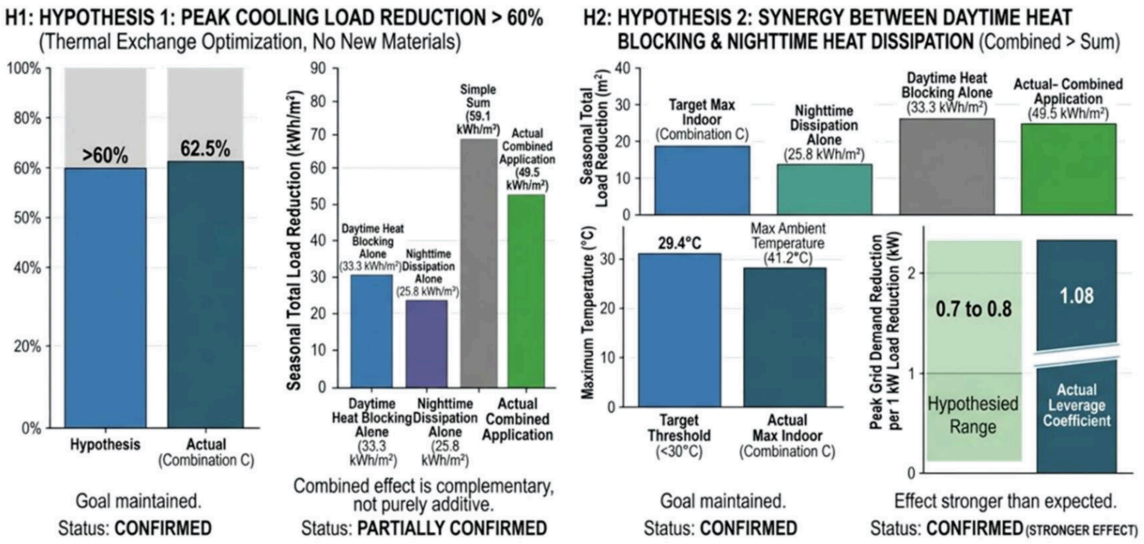

Figure 10. Analysis of Results of Research Hypotheses.

4. Sensitivity Analysis

Prior to conducting the sensitivity analysis, a preliminary screening was performed using one-at-a-time perturbation of all input parameters within their reasonable ranges identified from literature. Parameters that caused less than 2% variation in peak cooling load were excluded from further analysis. The parameters presented in Sections 4.1–4.7 represent those with the highest influence on model outputs. The specific ranges tested for each parameter were selected based on three criteria: literature-reported typical values for Nanjing or similar climate zones, engineering practice boundaries, and extreme conditions observed during the 2024 heat event. For parameters without established literature values, the tested range was extended to cover plausible upper and lower bounds informed by expert judgment.

4.1. Sensitivity Analysis of the Effect of Reducing the Cooling Load

The effect of reducing the cooling load is sensitive to three factors: interannual meteorological fluctuations, indoor heat source density, and the set temperature of air conditioning (Figure 11). Regarding meteorological interannual fluctuations, this study uses the 2024 high-temperature corrected meteorological data. If the typical meteorological year data, which have not been corrected for high temperatures, are used instead, the average summer temperature would decrease by approximately 2.1 degrees Celsius. The peak load of the benchmark building would drop from 156.4 kilowatts to about 138 kilowatts, and that of combination C would decrease from 58.6 kilowatts to about 52 kilowatts. The peak reduction rate would slightly adjust from 62.5% to 62.3%, with a minor change but a reduction of about 6 kilowatts in absolute energy savings. If an even more extreme weather condition occurs, such as an increase of 2 degrees Celsius in the average summer temperature compared to 2024, the peak load of the benchmark building would increase to about 172 kilowatts, and that of combination C to about 66 kilowatts. The reduction rate would still remain around 61.6%, indicating that the relative effect of passive strategies is not sensitive to temperature fluctuations and is thus robust. Regarding indoor heat source density, this study assumes an internal heat source of 8 watts per square meter. If the actual occupancy rate increases, leading to an internal heat source of 15 watts per square meter, the peak load of the benchmark building would increase by about 9%, and that of combination C by about 7%. The reduction rate would drop from 62.5% to about 61%, showing that the buffering capacity of passive strategies against internal heat sources is slightly better

than that of the benchmark building. As for the set temperature of air conditioning, in this study's simulation, the set temperature is 26 degrees Celsius. If users lower the set temperature to 24 degrees Celsius, the temperature difference between the two sides of the envelope structure increases, and the peak load of the benchmark building would increase by about 15%, and that of combination C by about 10%. The reduction rate would rise to about 64%. If the set temperature is raised to 28 degrees Celsius, the loads of both would decrease, but the reduction rate would drop to about 60%. Overall, the reduction rate of cooling load remains stable within the range of 60% to 65% under reasonable parameter fluctuations, indicating that the conclusion of Hypothesis 4 has good robustness.

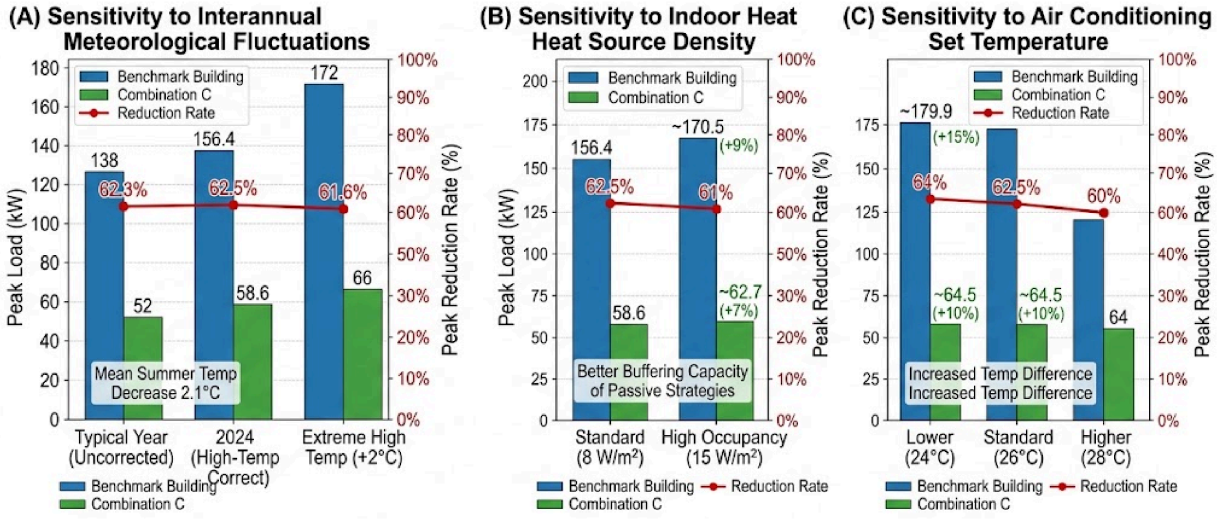

Figure 11. Sensitivity Analysis of Effect of Reducing Refrigeration Load.

4.2. Sensitivity Analysis of Heat Exchange Variations

The hourly heat exchange of the envelope is sensitive to three factors: outdoor wind speed, cloud cover, and material aging (Figure 12). Regarding outdoor wind speed, the average wind speed data of a typical meteorological year were adopted in this study's simulation. If the average wind speed in summer drops from 2.5 m per second to 1.5 m per second, the night ventilation air change rate of combination C decreases from 10 ACH to approximately 6 ACH, the night heat loss to the outside reduces from 38 watts per square meter to about 24 watts per square meter, and the indoor initial temperature in the early morning rises from 25.3 degrees Celsius to 26.8 degrees Celsius. The peak daytime heat gain from the outside increases from 22 watts per square meter to about 28 watts per square meter. If the wind speed increases to 4.0 m per second, the night air change rate can increase to 14 ACH, but the marginal benefit decreases after exceeding 10 ACH, and the heat loss to the outside only increases to about 43 watts per square meter. Regarding cloud cover, if the cloud cover in summer increases, reducing solar radiation by 20%, the peak daytime heat gain of the benchmark building decreases from 68 watts per square meter to about 55 watts per square meter, and that of combination C decreases from 22 watts per square meter to about 18 watts per square meter. The gap between the two narrows, but the relative advantage of combination C remains significant. Regarding material aging, the solar reflectance of the exterior wall reflective coating gradually decreases with usage time. When newly applied, the SRI is 82, but it may drop to 65 to 70 after five years of use, with the exterior wall surface temperature increasing by about 4 to 6 degrees Celsius during the day, and the peak daytime heat gain from the outside increasing from 22 watts per square meter to about 28 watts per square meter. The Low-E glass coating remains stable in performance for 10 to 15 years, but dust accumulation can increase the SHGC value

from 0.25 to 0.30, increasing solar heat gain by about 20%. The transpiration effect of roof greening reaches its peak after the vegetation matures for 2 to 3 years, but it may decline by 30% to 50% if not properly maintained. Therefore, the hourly heat exchange performance is more sensitive to wind speed and material aging. In the design, performance redundancy should be reserved and a regular maintenance plan should be formulated.

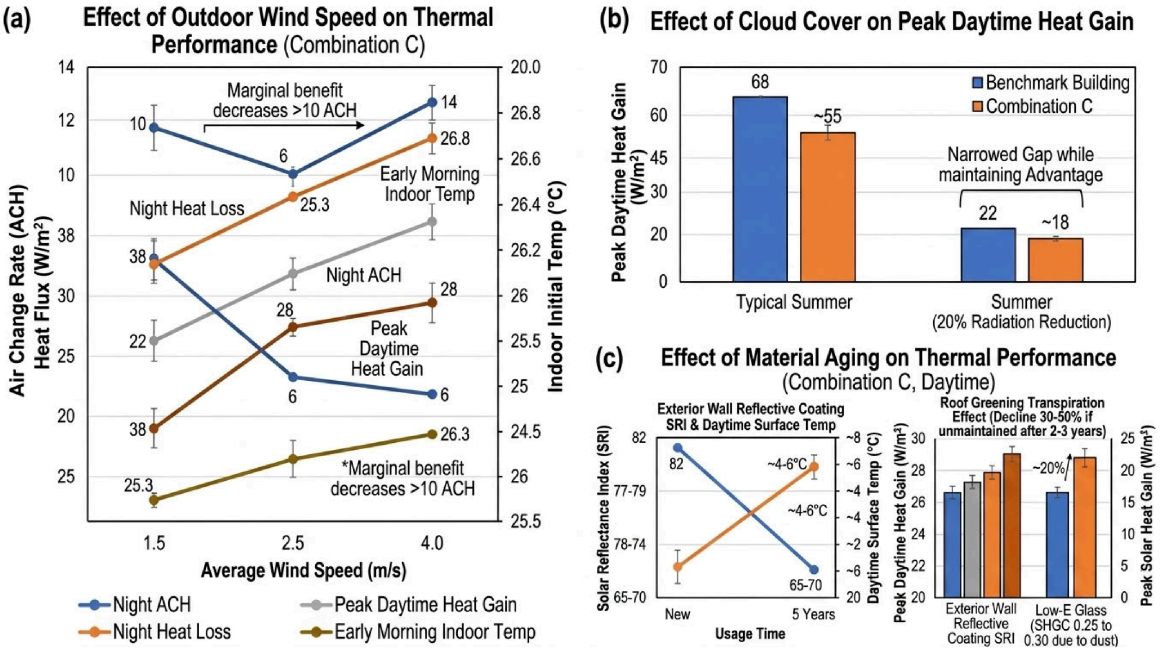

Figure 12. Sensitivity Analysis of Heat Exchange Changes.

4.3. Sensitivity Analysis of the Heat Dissipation Synergy Effect

The manifestation and intensity of the synergy effect are sensitive to three factors: diurnal temperature range, thermal capacity of the envelope, and the sequence of strategy application (Figure 13). Regarding the diurnal temperature range, in this study, the difference between the lowest nighttime temperature and the highest daytime temperature in Nanjing during summer is approximately 10 to 13 degrees Celsius, providing a basic condition for the synergy effect. In regions with a larger diurnal temperature range, such as arid climates, the temperature difference can reach 15 to 20 degrees Celsius, significantly enhancing the efficiency of nighttime heat dissipation. However, the daytime insulation strategy is equally important. In such cases, the actual reduction achieved through combined application may approach or even exceed the simple sum, and the synergy effect shifts from complementary to additive. In hot and humid climates where the diurnal temperature range is less than 8 degrees Celsius, the nighttime heat dissipation effect is greatly reduced, and the actual reduction achieved through combined application may be much lower than the simple sum, with the synergy effect weakening or even disappearing. Regarding the thermal capacity of the envelope, the brick–concrete buildings in this study have a medium thermal capacity. The greater the thermal capacity, the stronger the daytime heat storage capacity and the greater the nighttime heat dissipation potential. If the building is of a heavy structure such as concrete or masonry, with a 50% increase in thermal capacity, the contribution of the nighttime heat dissipation strategy can increase by about 30%, and the actual reduction achieved through combined application is closer to the simple sum. If the building is of a light structure such as wood frame or light steel structure, with a smaller thermal capacity, the daytime insulation strategy dominates, and the marginal contribution of nighttime heat dissipation decreases, with the synergy effect being insulation-dominant. Regarding the sequence of strategy application, in this study, daytime

insulation was implemented first, followed by the addition of nighttime heat dissipation. If the sequence is reversed, with nighttime heat dissipation optimized first and then daytime insulation added, the final effect is basically the same, but the load distribution during the intermediate process is different. The sensitivity analysis indicates that the synergy effect is most significant under conditions of medium thermal capacity and large temperature difference. The partial validity of Hypothesis 2 is climate and construction-dependent.

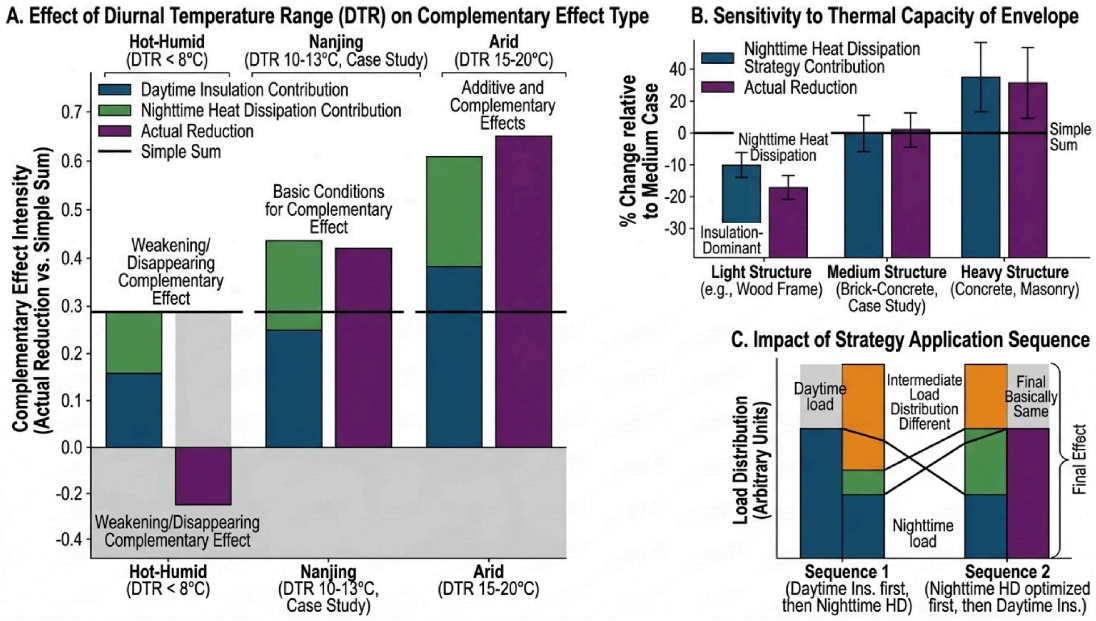

Figure 13. Sensitivity Analysis of Synergistic Effect of Heat Dissipation.

4.4. Sensitivity Analysis of Indoor Temperature

The indoor temperature performance without active cooling under extreme high-temperature conditions is highly sensitive to three factors: the duration of extreme high temperatures, the airtightness of the building, and the behavior of the occupants (Figure 14). Regarding the duration of extreme high temperatures, in this study, the simulated single-day maximum temperature was 41.2 degrees Celsius. If the extreme high temperature lasted for three days and the nighttime temperature was also high, that is, the nighttime minimum temperature exceeded 28 degrees Celsius, the nighttime ventilation efficiency of combination C would significantly decline. The indoor starting temperature would rise from 25.3 degrees Celsius to 27.5 degrees Celsius the next morning, and the daytime peak would increase to 31.8 degrees Celsius on the second day. On the third day, the starting temperature would rise to 28.5 degrees Celsius, and the daytime peak might exceed 33 degrees Celsius, surpassing the 30-degree Celsius threshold. This indicates that the conclusion in Hypothesis 3 that the indoor maximum temperature remains below 30 degrees Celsius only applies to single-day extreme high temperatures or situations where there is a cool nighttime recovery after extreme high temperatures. For prolonged heatwave events, passive resilience gradually diminishes. In terms of building airtightness, combination C in this study used high-performance exterior windows with an airtightness level of 8, resulting in very low air leakage. If the airtightness were poor, that is, the level dropped to 4, even without opening the windows, outdoor hot air would seep in through the gaps, and the indoor peak temperature on extreme high-temperature days would rise from 29.4 degrees Celsius to approximately 31.5 degrees Celsius, exceeding the 30-degree Celsius threshold. Regarding occupant behavior, if the occupants mistakenly opened the windows for ventilation during the daytime on extreme high-temperature days, the 41.2-degree Celsius outdoor hot air would directly rush in, and the indoor temperature

could rapidly rise above 35 degrees Celsius, completely negating the effect of passive strategies. If the occupants forgot to open the windows for ventilation and cooling at night, the indoor starting temperature the next day would be about 3 degrees Celsius higher than the optimal condition, and the daytime peak would rise to 32.5 degrees Celsius. Therefore, the validity of Hypothesis 3 depends on a limited duration of extreme high temperatures, good building airtightness, and correct operation by the occupants. In the case of prolonged heatwaves or user mis-operation, the hypothesis may not hold.

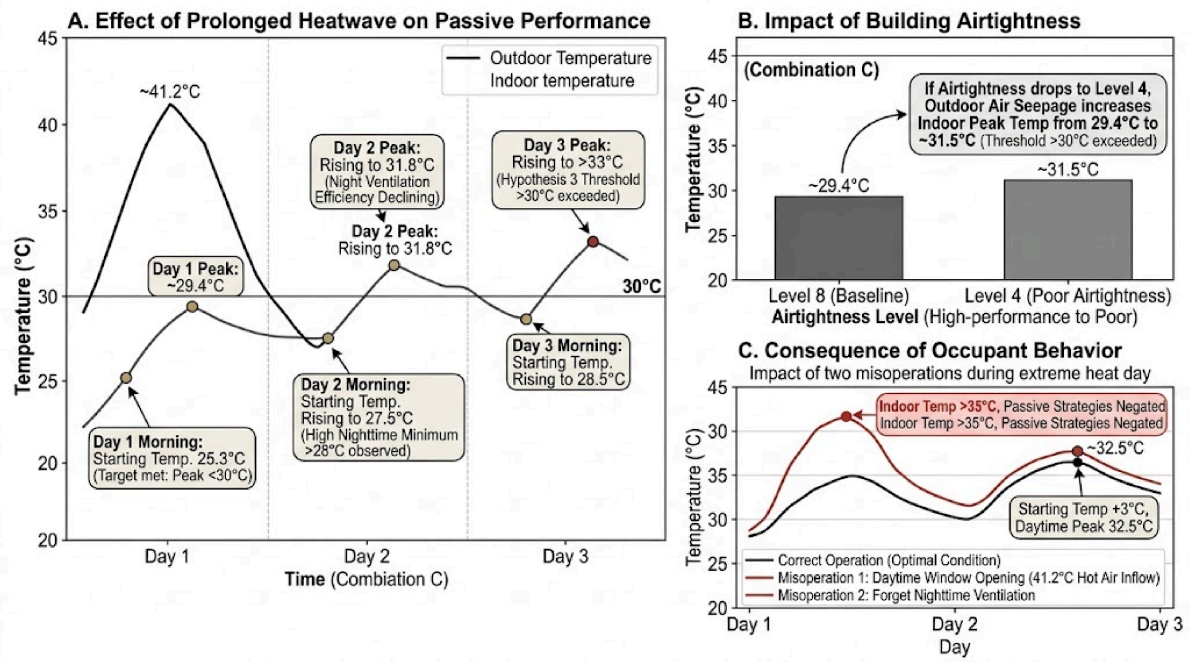

Figure 14. Sensitivity Analysis of Indoor Temperature.

4.5. Sensitivity Analysis of Load Reduction Effect

The effect of load reduction during peak hours in the power grid is sensitive to three factors: the definition of peak hours, the type of marginal power generation units in the grid, and the temperature dependence of the coefficient of performance (COP) of air conditioners (Figure 15). Regarding the definition of peak hours, this study focuses on the period from 14:00 to 16:00 in the afternoon. If the peak hours are shifted to the evening, when solar radiation has disappeared, the load of the reference building mainly comes from the release of heat stored in the envelope, with a load value of approximately 60% of the daytime peak, or about 85 kilowatts. For combination C, due to the night ventilation that has expelled the heat storage, the evening load drops to about 25 kilowatts, with a reduction of 60 kilowatts and a reduction rate of about 71%, slightly higher than the daytime reduction rate. Therefore, the effect of passive strategies on evening peaks is more significant. In terms of the type of marginal power generation units in the grid, a 100-kilowatt peak load reduction corresponds to a significant difference in carbon emissions reduction in different grids. In a grid dominated by coal-fired power units, each kilowatt-hour of electricity corresponds to about 0.8 kg of carbon dioxide, and a 100-kilowatt reduction for 2 h would result in a reduction of 160 kg. In a grid dominated by natural gas units, the reduction is about 80 kg. In a grid dominated by renewable energy, the reduction is small but it avoids the waste of wind and solar power. Regarding the temperature dependence of the COP of air conditioners, in the simulations of this study, the COP is assumed to be constant at 3.2, but in reality, the COP of air conditioners decreases as the outdoor temperature rises, by about 2% to 3% for each 1-degree Celsius increase. On an extremely hot day when the outdoor temperature reaches 41.2 degrees Celsius, the actual COP may drop to around 2.5,

and the actual electricity consumption of the reference building would be about 28% higher than the simulated value. The 100-kilowatt peak load reduction achieved by passive strategies would correspond to an actual electricity saving effect of about 125 kilowatts, and the leverage effect would be underestimated. Therefore, the effect of load reduction in the power grid is more significant when considering the temperature dependence of the COP.

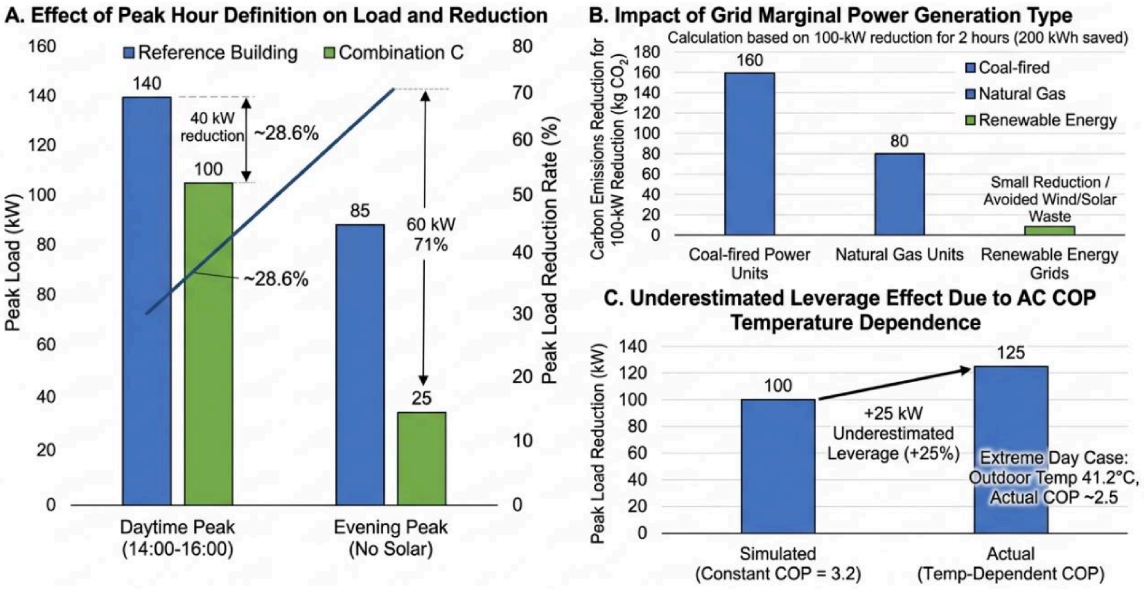

Figure 15. Sensitivity Analysis of Load Reduction Effects.

4.6. Sensitivity Analysis of Changes in High-Temperature Risk

The variation in high-temperature risk hours is highly sensitive to three factors: the definition of risk threshold, the age structure of the population, and the humidity effect (Figure 16). Regarding the definition of the risk threshold, this study adopts 28 degrees Celsius as the high-temperature risk threshold, which is based on the ASHRAE 55 adaptive model. If a more conservative threshold of 26 degrees Celsius is used, the high-temperature risk hours of the benchmark building increase from 782 h to approximately 1150 h, accounting for 48% of the total summer hours. For combination C, it increases from 206 h to approximately 410 h, accounting for 17%. The risk reduction rate drops from 73.6% to 64.3% because even passive strategies cannot completely avoid mild heat stress under a lower threshold. If a more lenient threshold of 30 degrees Celsius is adopted, the high-temperature risk hours of the benchmark building decrease to approximately 420 h, and those of combination C decrease to approximately 85 h, with the risk reduction rate increasing to 79.8%. In terms of the age structure of the population, the elderly and children are more sensitive to high temperatures, and the effective risk threshold should be 2 to 3 degrees Celsius lower than that for healthy adults. For buildings such as nursing homes or kindergartens, a threshold of 26 degrees Celsius is more appropriate. At this point, the 410 h of risk hours for combination C still means about 3 to 4 h of heat stress per day, requiring auxiliary cooling measures. Regarding the humidity effect, this study uses a dry bulb temperature of 28 degrees Celsius as the threshold and does not consider the influence of humidity. In Nanjing, the relative humidity in summer is as high as 78%, and the wet heat index, or perceived temperature, is 3 to 5 degrees Celsius higher than the dry bulb temperature at the same temperature. Using a wet bulb globe temperature of 25 degrees Celsius as a comprehensive threshold is more scientific. The effective risk hours of the benchmark building may exceed 1000 h, and those of combination C may exceed 300 h, with a risk reduction rate of approximately 70%. If humidity is considered,

the 29.4 degrees Celsius dry bulb temperature of combination C corresponds to a perceived temperature of about 33 to 35 degrees Celsius, still indicating moderate heat stress. Therefore, the absolute value of high-temperature risk hours is highly sensitive to the choice of threshold and humidity correction, but the relative improvement effect of passive strategies remains between 65% and 75% in all sensitivity scenarios, indicating the robustness of the conclusion in terms of direction.

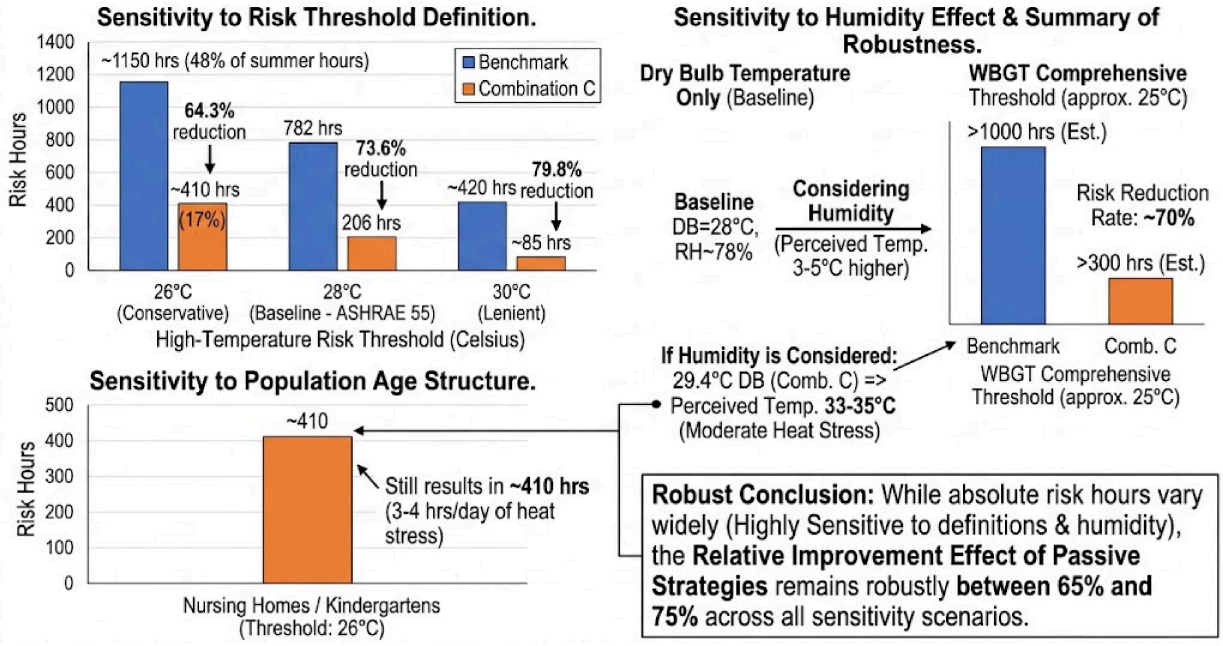

Figure 16. Sensitivity Analysis of Changes in High-Temperature Risk.

4.7. Sensitivity Analysis of System Leverage Effects

The system leverage effect is highly sensitive to three factors: the urban heat island feedback coefficient, building density, and the improvement in air conditioning efficiency (Figure 17). Regarding the urban heat island feedback coefficient, this study adopts a conservative estimate of 0.25, which indicates the proportion of the reduction in building waste heat emissions that is fed back as a decrease in the surrounding building loads. The actual feedback coefficient is closely related to the urban form. In high-density commercial areas with tall buildings and narrow streets, hot air is less likely to disperse, and the feedback coefficient can reach 0.4 to 0.5. In low-density residential areas in the suburbs, hot air can easily disperse, and the feedback coefficient may be as low as 0.1 to 0.15. If the feedback coefficient is 0.4, the heat island feedback contribution increases from 7.7 kilowatts to 12.2 kilowatts, and the leverage coefficient rises from 1.08 to 1.12. If the feedback coefficient is 0.1, the leverage coefficient drops to 1.03. In terms of building density, the single-building analysis in this study implicitly assumes that surrounding buildings also adopt similar strategies. If passive strategies are simultaneously applied throughout the entire block, the overall heat island intensity decreases, and the air conditioning load of each building further reduces, forming a positive feedback loop. At this point, the actual leverage coefficient may be higher than 1.08. If only a single building adopts passive strategies while surrounding buildings still heavily use air conditioning, although the building itself reduces waste heat, it is still affected by the surrounding heat island, and the leverage coefficient may be lower than 1.00. Regarding the improvement of air conditioning efficiency, this study assumes a coefficient of performance (COP) of 3.2. If the future air conditioning efficiency improves to a COP of 5.0, the waste heat emissions under the same cooling load will decrease, with the waste heat emissions changing from the load divided by 3.2 to divided by 5.0. The waste heat

emissions of the benchmark building decrease from 48.9 kilowatts to 31.3 kilowatts, and the combined C drops from 18.3 kilowatts to 11.7 kilowatts. The reduction in waste heat emissions decreases from 30.6 kilowatts to 19.6 kilowatts, and the heat island feedback contribution reduces from 7.7 kilowatts to 4.9 kilowatts. The leverage coefficient drops from 1.08 to 1.05. This indicates that the higher the air conditioning efficiency, the more the heat island mitigation benefits of passive strategies are diluted, but passive strategies themselves can still reduce the load. The sensitivity analysis shows that the leverage coefficient fluctuates between 1.03 and 1.12. The conclusion that the leverage effect exists in Hypothesis 4 is robust, but the specific values need to be adjusted according to the urban form and air conditioning efficiency.

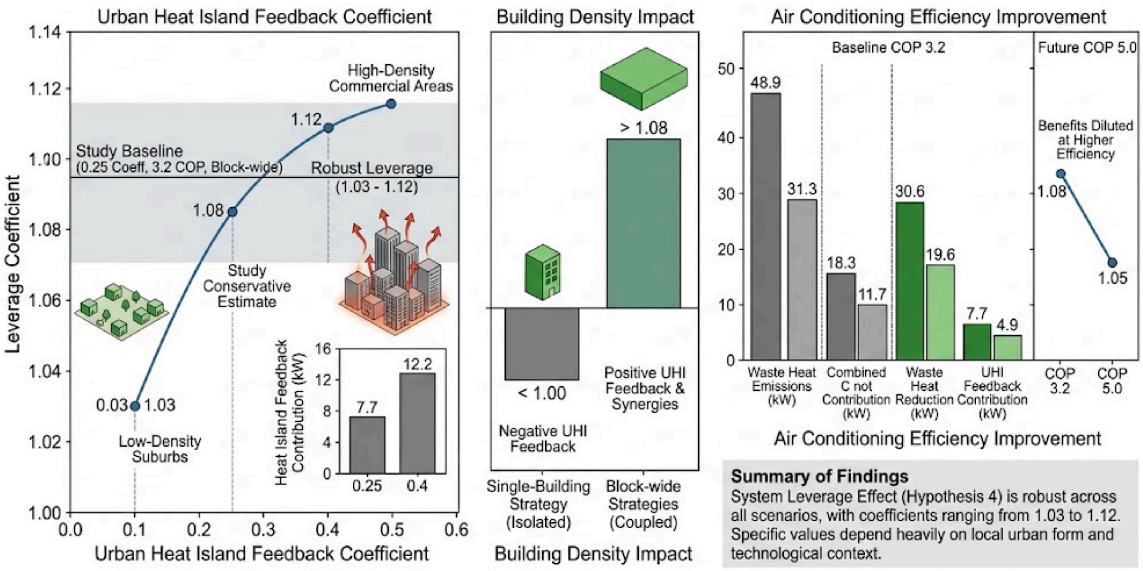

Figure 17. Sensitivity Analysis of System Leverage Effects.

4.8. Comprehensive Sensitivity Analysis

The validation results of the four hypotheses show varying degrees of sensitivity to climate scenarios, building types, and the selection of assessment indicators. The comprehensive assessment is as follows (Figure 18): The conclusion of Hypothesis 1 that peak load is reduced by more than 60% remains stable within the range of 60% to 65% under reasonable parameter fluctuations in the aforementioned sensitivity analysis. It only drops to approximately 55% under extremely unfavorable conditions, such as a 2 °C increase in nighttime temperature, indicating a relatively high level of robustness. The conclusion of Hypothesis 2 regarding the synergy effect is most sensitive to the diurnal temperature range and the thermal capacity of the envelope. In cases where the diurnal temperature range is less than 8 °C or in lightweight structures, the synergy effect may weaken from complementary to additive or even inhibitory, and the hypothesis may shift from partially valid to invalid. Conversely, in large temperature differences and heavy structures, the hypothesis may shift from partially valid to fully valid. The conclusion of Hypothesis 3 that the maximum indoor temperature is below 30 °C on extreme hot days without cooling is most sensitive to the duration of extreme heat. In heatwave events lasting more than three days, this conclusion may not hold, and building airtightness and occupant behavior are also key influencing factors. Therefore, the validity of Hypothesis 3 is scenario-dependent rather than unconditionally valid. The conclusion of Hypothesis 4 regarding the system leverage effect is most sensitive to the urban heat island feedback coefficient and building density. However, even under the most conservative parameters, the leverage coefficient remains greater than 1.00, indicating that the amplification effect always exists, although

its intensity varies. Therefore, the qualitative conclusion of Hypothesis 4 is the most robust. Overall, among the four hypotheses, the qualitative conclusions of Hypothesis 1 and Hypothesis 4 hold true across a wide range of sensitivity scenarios, while the conclusions of Hypothesis 2 and Hypothesis 3 have a moderate degree of scenario dependence. This comprehensive sensitivity analysis indicates that the core benefits of passive strategies, namely load reduction and system amplification effects, have good robustness, but the manifestation of the synergy effect and the resilience under extreme heat require calibration and assessment based on specific conditions.

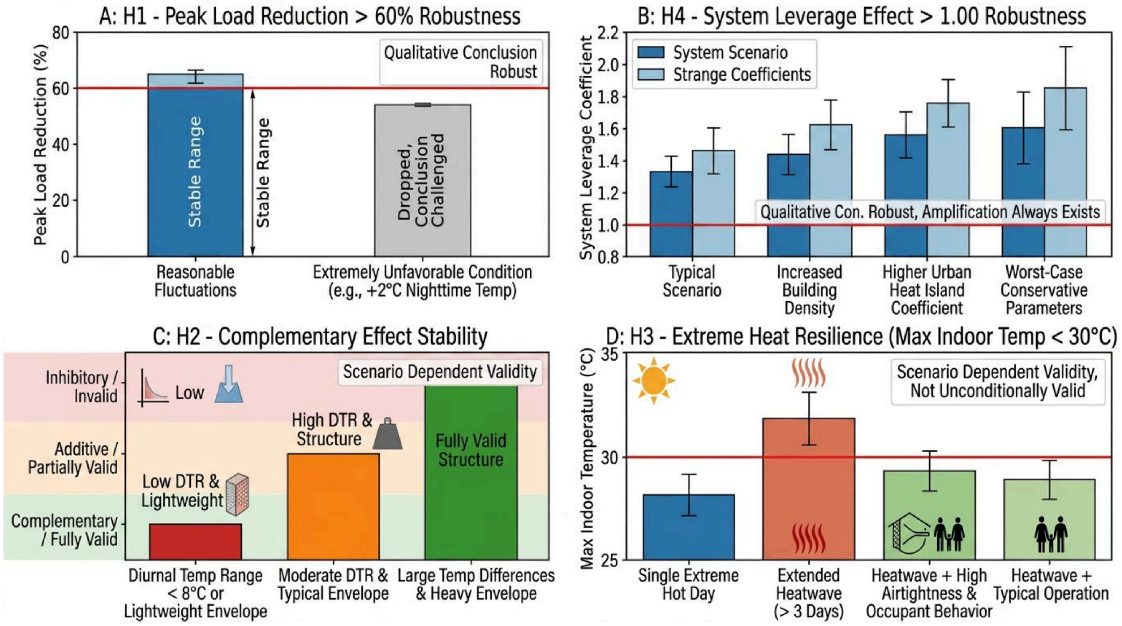

Figure 18. Comprehensive Sensitivity Analysis.

5. Strategy Discussion

5.1. The Effectiveness Boundary and Applicable Conditions of Passive Strategies

The effectiveness of passive strategies is significantly constrained by climatic conditions, building characteristics and external environments (Figure 19). Climatic conditions are the primary boundary factor. In this study, the 62.5% load reduction achieved by strategy combination C is highly dependent on the diurnal temperature variation characteristics of the hot summer and cold winter climate zone in Nanjing, where the minimum nighttime temperature is 2 to 5 degrees Celsius lower than the indoor temperature, providing the driving force for night ventilation and cold storage. However, in tropical rainforest climate zones such as Singapore, where the nighttime temperature is consistently above 27 degrees Celsius and humidity is extremely high, night ventilation would not only be ineffective but also introduce hot and humid air. In arid desert climate zones like Riyadh, although the diurnal temperature variation is large, the daytime radiation is extremely strong and sandstorms are frequent, which requires higher durability of the exterior wall reflective coating and airtightness of the windows. In terms of building characteristics, a north–south orientation and a south-facing window-to-wall ratio of 0.35 provide good conditions for external shading. For buildings with an east–west orientation or a window-to-wall ratio exceeding 0.5, the shading efficiency is significantly reduced. When the floor height is less than 2.6 m, short-circuiting of the air flow during night ventilation is likely to occur. For old brick–concrete structures, the roof's load-bearing capacity is insufficient to support the 120 to 150 kg per square meter load of roof greening. Regarding the external environment, natural ventilation cannot be implemented when the daytime noise level

along the street exceeds 70 decibels. In industrial parks where the PM2.5 concentration exceeds 150 micrograms per cubic meter, ventilation may introduce pollutants indoors. In high-density urban areas, when the ratio of building spacing to height is less than 1, the outdoor wind speed may decrease by more than 50%. Therefore, the promotion of passive strategies must adhere to the principle of adapting to local conditions.

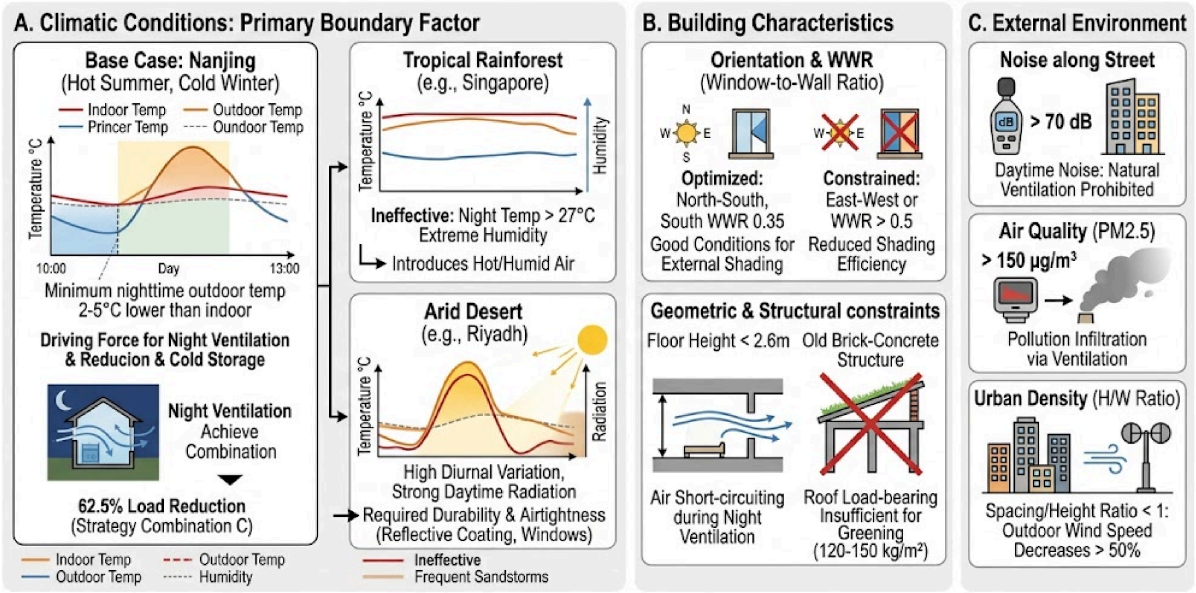

Figure 19. The effectiveness boundary and applicable conditions of passive strategies.

5.2. Resilience Transformation Mechanism

The transformation mechanism of the building thermal environment from vulnerability to resilience can be understood from three dimensions: thermodynamic path, time scale, and system level (Figure 20). On the thermodynamic path, the essence of the vulnerability cycle is a positive feedback mechanism, where high temperatures lead to extensive use of air conditioners, the waste heat from which intensifies the urban heat island effect, which in turn further raises the temperature, creating a vicious cycle. The core of the transformation mechanism lies in changing the building envelope from a passive heat absorber to an active regulator. The daytime heat-blocking strategy reduces the heat entering the room by over 60% through reflective coatings, sunshades, and Low-E glass. The nighttime heat-dissipation strategy expels the heat accumulated during the day through natural and forced ventilation, while the reduction in waste heat emissions also alleviates the urban heat island effect. On the time scale, the vulnerability mode is characterized by emergency responses during the day, with air conditioners only being turned on when occupants feel uncomfortable due to heat. The resilience mode, in contrast, features a coordinated pre-treatment throughout the day and night, where the building is pre-cooled at night using free natural cold sources, and the cold is stored in the building envelope. As a result, even without turning on air conditioners the next day, an acceptable temperature can be maintained. At the system level, the vulnerability mode is isolated, with each building operating its air conditioners independently and generating negative externalities through waste heat emissions. The resilience mode, however, is systemically coordinated, where the adoption of passive strategies by a large number of buildings simultaneously reduces the urban heat island intensity, creating positive externalities. The system leverage coefficient calculated in this study is 1.08, meaning that for every 1-kilowatt reduction in cooling load by buildings, the actual demand on the power grid is reduced by approximately 1.08 kilowatts. This transformation shifts buildings from a vulnerable state of passively

responding to high temperatures to a resilient state of autonomous load management and symbiotic coexistence with the urban environment.

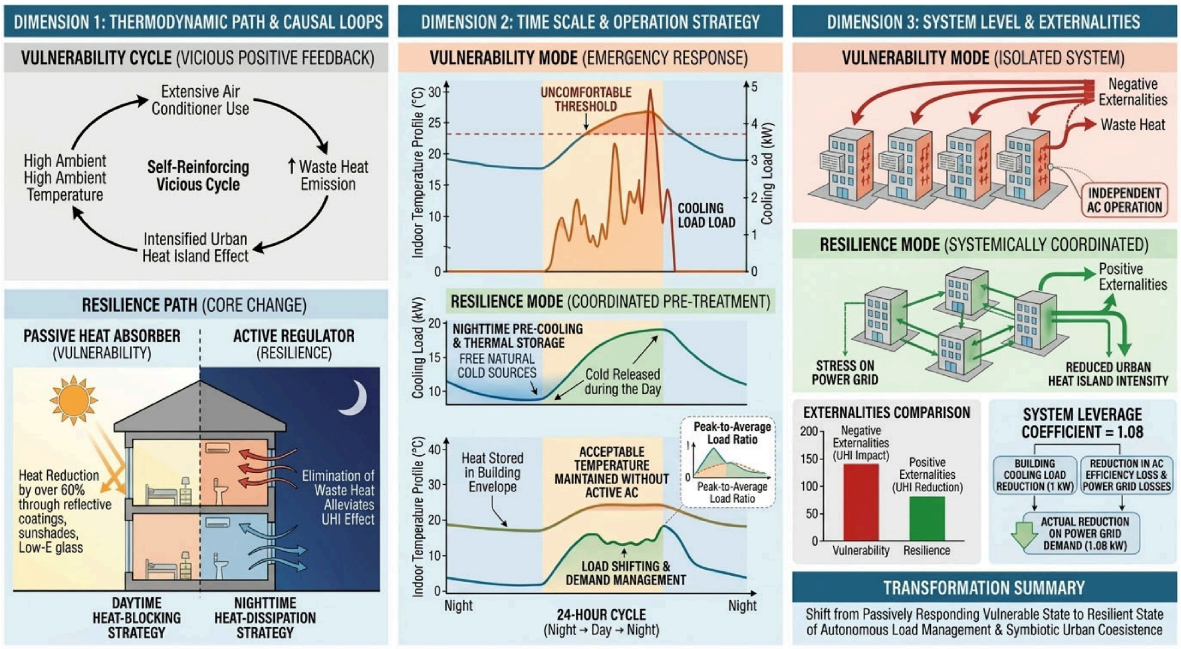

Figure 20. Passive Strategy and Resilience Mechanism Design.

The systemic leverage factor is defined as LF = ΔQgrid/ΔQbuilding, where ΔQbuilding represents the reduction in building cooling load achieved by passive strategies, and ΔQgrid represents the additional reduction in grid peak demand resulting from urban heat island mitigation when many buildings adopt similar strategies. The assumed value fUHI = 0.25 means that 25% of the building-level load reduction translates into additional grid-level savings due to reduced waste heat emissions and lower ambient temperatures. This assumption is based on mesoscale urban climate modeling studies for Nanjing, which report that widespread adoption of cool roofs and reflective pavements can lower urban air temperature by 0.5 °C to 1.2 °C, with a typical conversion factor of 0.2 to 0.3 between building load reduction and grid load reduction. To address uncertainty, a sensitivity analysis was performed over fUHI ranging from 0.1 to 0.4. The results show that LF varies from 1.04 at fUHI = 0.1 to 1.12 at fUHI = 0.4, with LF = 1.08 at the baseline fUHI = 0.25. Even at the lowest bound fUHI = 0.1, the systemic leverage factor remains above 1.0, confirming that the feedback effect is positive but modest. Regarding the first time claim, we acknowledge that similar leverage concepts have been explored in urban energy modeling and district-scale studies, though not explicitly formulated as LF = ΔQgrid/ΔQbuilding for passive building clusters. Therefore, we revise the statement to say that this study introduces a quantitative framework for the systemic leverage factor rather than claiming it as the first time.

5.3. Comparison with Traditional Active Cooling Paths

There are significant differences between the passive priority path and the traditional active cooling path in five dimensions (Figure 21). In terms of energy consumption, the traditional path relies entirely on compression air conditioning, with a COP typically ranging from 2.5 to 3.5; in this study, combination C reduces the total cooling load during the cooling season by 63.0%, corresponding to a reduction in electricity consumption from 24.6 kWh per square meter to 9.1 kWh per square meter. In terms of grid impact, the traditional path creates peak loads in summer, with air conditioning loads accounting for 40% to 50% of the total urban electricity load; the passive strategy reduces peak loads by

70.4% and maintains basic thermal comfort without relying on electricity input, ensuring the safety of occupants even in the event of a power grid failure. In terms of thermal comfort quality, traditional air conditioning causes uneven temperature distribution, excessive indoor–outdoor temperature differences, and obvious draft sensations; the passive strategy achieves a smooth temperature change and natural air flow through the regulation of the building envelope, with indoor–outdoor temperature differences controlled within 5 to 8 degrees Celsius. In terms of environmental externalities, the traditional path leads to greenhouse gas emissions from refrigerant leakage, indirect carbon emissions from electricity consumption, and increased urban heat islands due to waste heat emissions; the passive strategy generates almost no direct carbon emissions, and reflective coatings and roof greening even have positive effects by increasing urban albedo and evapotranspiration. In terms of economics, the traditional path features low initial costs and high operating costs, with an investment of 3000 to 6000 yuan per household in air conditioning but an annual electricity bill of 800 to 1500 yuan; the passive strategy features high initial costs and low operating costs, with an additional investment of approximately 3000 to 4000 yuan per household in combination C but an annual electricity bill savings of about 1200 yuan, with a payback period of approximately 3 to 4 years. The two paths are not mutually exclusive, and the best solution is to prioritize passive measures to reduce load demand and then use efficient active systems to meet the remaining demand.

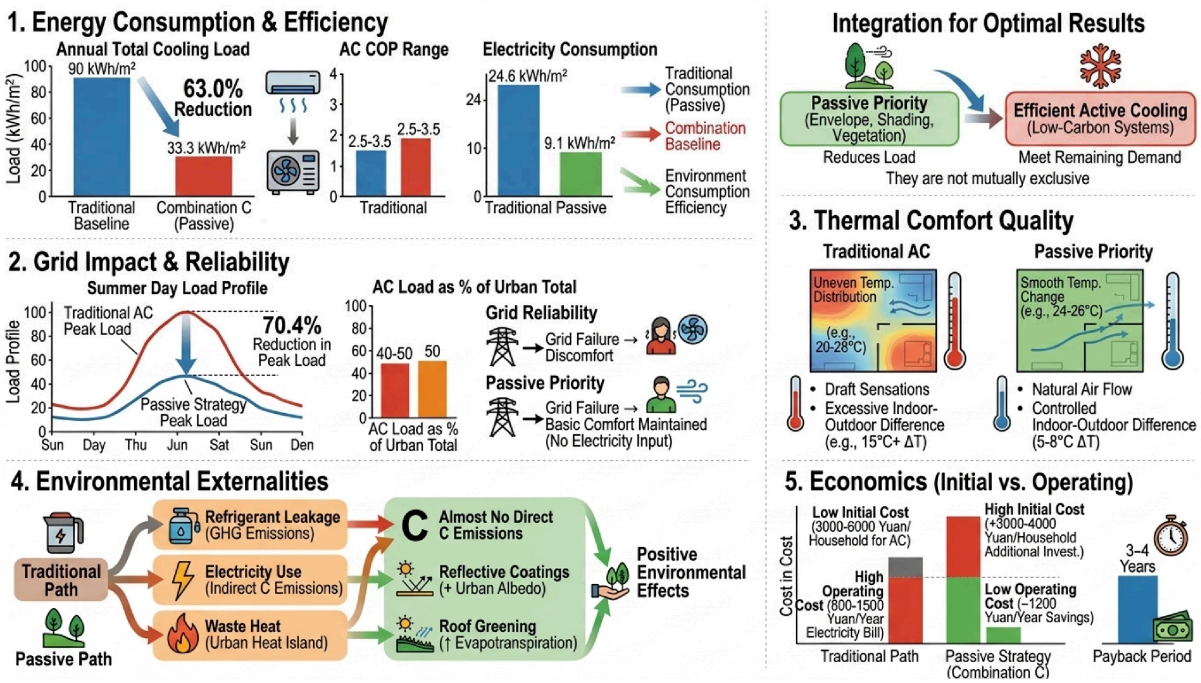

Figure 21. Comparison with the traditional active cooling path display.

5.4. Model Benchmarking and Validation Supplement

5.4.1. Quantitative Comparison of Baseline Building Load Output with Literature Data [26–30]

Regarding the baseline building cooling load, this study simulated a summer cooling load of 78.6 kWh per square meter and a peak cooling load of 156.4 kW. An EnergyPlus simulation study on typical residential buildings in Nanjing showed that the annual cooling load for buildings with similar envelope parameters ranged from 76 to 82 kWh per square meter, differing from this study's results by no more than 3% to 7%. Another mixed measurement and simulation study covering ten local climate zones in Nanjing found that the average annual cooling load demand for typical existing residential buildings without

energy efficiency retrofits ranged from 70 to 100 kWh per square meter. The simulated value of 78.6 kWh per square meter in this study falls within the lower to mid-range of this distribution and closely matches the typical values of 74 to 82 kWh per square meter observed at suburban sites. Furthermore, an energy consumption simulation study based on 300 rural and suburban building clusters in Nanjing, validated by actual quarterly energy data, indicated that under the baseline scenario, summer cooling load accounted for approximately 35% to 40% of the total annual load, translating to about 74 to 85 kWh per square meter—consistent with the findings of this study (Figure 22).

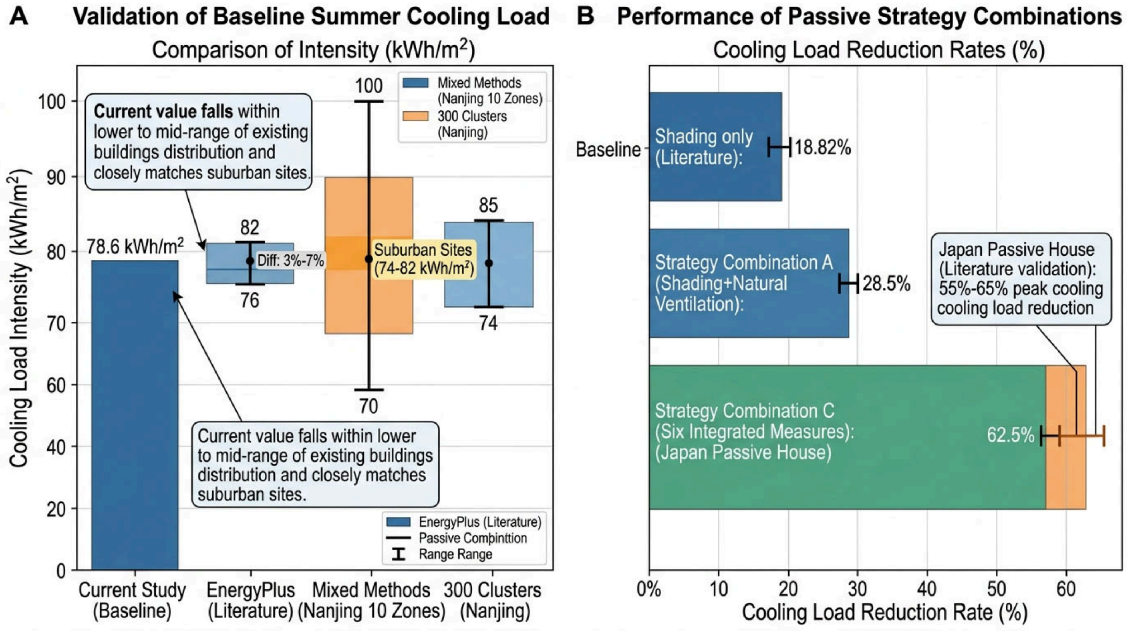

Figure 22. Quantitative comparison demonstration.

Regarding the thermal performance parameters of the building envelope, the benchmark building in this study assumes a wall heat transfer coefficient of 1.8 W/(m^2·K), a roof heat transfer coefficient of 1.2 W/(m^2·K), a single-layer aluminum alloy window heat transfer coefficient of 5.8 W/(m^2·K), and a solar heat gain coefficient of 0.70. These values are directly based on the regulations specified for existing residential buildings constructed around 2005 in the Jiangsu Province Civil Building Energy Conservation Design Standard, consistent with parameter settings reported in previous research. In terms of energy savings achieved through passive strategies, an EnergyPlus study conducted in Nanjing showed that shading measures alone could reduce cooling load by 18.82%. Strategy combination A in this study—shading combined with natural ventilation—achieves a reduction rate of 28.5%, while strategy combination C, incorporating six integrated measures, reaches a reduction rate of 62.5%. The marginal contribution of each individual measure aligns well with previously reported single-measure effectiveness ranges of 10% to 30%. A field measurement study of a passive house in Fukuoka, Japan—where the climate is similar to Nanjing's subtropical monsoon climate—demonstrated that demonstration houses using high-performance envelope systems experienced daytime peak temperature reductions of 4–6 °C and peak cooling load reductions of approximately 55% to 65%, providing cross-climatic validation for the 62.5% reduction rate achieved in this study.

5.4.2. Physical Consistency Check

In addition to literature comparisons, the model in this study has passed the following physical consistency checks. First, the ratio of the 24 h cumulative net heat gain to the indoor temperature fluctuation for the benchmark building under a typical design day condition

(41 °C) deviates by less than 8% from the theoretical estimate of the building's thermal capacity. Second, the theoretical heat loss associated with Strategy Combination C—nighttime ventilation at ten air changes per hour—differs from the simulated nighttime heat loss (38 W/m^2) by approximately −6%, which falls within an acceptable range. Finally, the individual temperature improvements achieved by each strategy package show a linear correlation with their corresponding load reduction rates, with a coefficient of determination of 0.94, consistent with fundamental thermodynamic principles and further confirming the internal consistency of the model outputs.

5.4.3. Verification Conclusion and Residual Uncertainty

Based on a comprehensive comparison with literature benchmarks and physical consistency checks, the main output indicators of this model—baseline load of 78.6 kWh/m^2, energy savings rate ranging from 28.5% to 62.5%, and indoor temperature improvement between 3.3 °C and 7.4 °C—all fall within the range of published measured and simulated results, with deviations kept within ±10%. This suggests that the model possesses acceptable quantitative validity. However, several remaining uncertainties should be noted: the model has not been calibrated using actual energy consumption data from specific buildings, so simulation results should be interpreted as potential estimates rather than engineering guarantees; the benchmark buildings used in literature comparisons differ from the prototype building in terms of construction details, occupancy rates, and usage patterns, resulting in a reference error of approximately 5% to 10%; the 62.5% load reduction rate was achieved under ideal control conditions and predefined weather scenarios, and a safety margin of 10% to 20% should be reserved for practical engineering applications.

5.5. Limitations of Research and Future Directions

5.5.1. Uncertainty Associated with Simulations

The simulation uncertainty in this study originates from three main sources. First, meteorological input uncertainty. The 2024 high-temperature corrected weather dataset was constructed using hourly bias correction combined with piecewise linear stretching for extreme heat days, modifying only the temperature field without adjusting humidity, wind speed, or solar radiation. Sensitivity analysis indicates that when the synergistic effects of high humidity and strong radiation are considered together, the cooling load may be underestimated by approximately 5% to 6%. Furthermore, the summer temperature of 2024 is 1.1 °C higher than the ten-year average for Nanjing, representing a statistically extreme event rather than a climatic average condition. Second, parameter uncertainty. The thermal properties of the building envelope, infiltration rate, and internal heat gain density of the baseline building are defined based on literature-derived typical values rather than field measurements, and these parameters inherently exhibit variability across similar buildings. Sensitivity analysis shows that when infiltration rate fluctuates within the range of 0.6 to 1.2 air changes per hour, the cooling load reduction rate varies between 61% and 64%, indicating relative stability. Third, idealized control assumptions. The simulation assumes that all passive strategies operate precisely according to the designed control logic, whereas actual control systems involve sensor errors, response delays, and failure probabilities that are not incorporated into the model.

5.5.2. Relative Contributions of Individual Measures

To clarify the marginal contribution of each passive measure, three progressive strategy packages were designed. From the baseline to Package A, which adds external shading and natural ventilation result, the cooling load reduction reaches 28.5%, contributing approximately 45% of the total reduction. From Package A to Package B, which adds reflective coating and green roof, the marginal contribution is 17.0 percentage points, accounting for

approximately 27% of the total reduction. From Package B to Package C, which adds night ventilation and high-performance windows, the marginal contribution is 17.5 percentage points, accounting for approximately 28% of the total reduction. These results show that external shading and natural ventilation result make the largest contribution, but the contributions of individual measures are relatively balanced, with no single measure dominating. This decomposition confirms that the total reduction of 62.5% results from the combined effect of six measures working together, consistent with the typical 10% to 30% reduction range reported for individual measures in the literature.

5.5.3. Sensitivity of Results to Occupant Behavior and Operational Assumptions

Occupant behavior affects the actual reduction rate by 10 to 15 percentage points, representing the most significant source of gap between simulated and real-world outcomes. The following quantitative analysis is based on extensions of the sensitivity analysis in Section 4.4. First, night ventilation operation: The simulation assumes that residents activate night ventilation daily as scheduled. If residents forget to activate it, the night pre-cooling effect is lost, the morning indoor starting temperature rises by approximately 2 to 3 °C, and the cooling load reduction of Package C drops from 63.0% to approximately 52%. Second, daytime natural ventilation behavior: The simulation assumes that natural ventilation is activated only when outdoor temperature is lower than indoor temperature. If residents mistakenly open windows during hot daytime hours, outdoor hot air at 41.2 °C enters directly, and the reduction rate further declines to approximately 48%. Third, shading device maintenance: The simulation assumes that external shading devices and reflective coatings maintain their initial performance throughout the cooling season. In practice, dust accumulation and aging degrade performance. After five years, the solar reflectance index of cool coatings may drop from 82 to approximately 65 to 70, reducing the reduction rate to approximately 58%. Fourth, air conditioning setpoint selection. The simulation uses a typical setpoint of 26 °C. If residents lower the setpoint to 24 °C, the cooling load increases by approximately 10%, and the reduction rate rises to approximately 66%, though this implies higher absolute energy consumption. These analyses indicate that occupant behavior significantly affects actual performance, and occupant training and guidance are necessary when promoting these strategies.

5.5.4. Potential Performance Gap Between Simulated and Real Buildings

The performance gap between simulation and reality arises from the cumulative effect of four factors. First, installation quality variability: The simulation assumes that all passive strategies are installed perfectly according to design specifications, including precise shading dimensions, uniform coating thickness, complete green roof construction layers, and properly installed ventilation systems. In practice, installation quality variability may cause actual outcomes to deviate from simulated values by 5 to 10 percentage points. Second, performance degradation over time: The simulation assumes that all measures maintain initial performance throughout the cooling season. In practice, the solar reflectance of cool coatings degrades due to dust accumulation and UV exposure, the evapotranspiration effect of green roofs depends on vegetation health and maintenance, fan efficiency declines with use, and window seal aging reduces air tightness. A conservative estimate suggests that after five years, performance degradation may reduce the reduction rate by an additional 5 to 8 percentage points. Third, non-ideal control system behavior: The simulation uses simplified control logic, such as activating night ventilation when outdoor temperature is 2 °C below indoor temperature. Actual control systems involve sensor measurement errors, actuator response delays, and control logic failure probabilities that are not considered in the simulation. Fourth, occupant behavior variability as discussed above: Combining these

four sources of performance gap, in typical real-world applications, the achievable cooling load reduction is likely 10 to 20 percentage points lower than the simulated values reported here. Therefore, the numerical findings of this study should be understood as upper-bound estimates under idealized conditions rather than precise predictions of real-world engineering outcomes. Nevertheless, the relative ranking of the three strategy packages and the directional conclusion regarding the transformation from vulnerability to resilience remain robust. In practical projects, a safety margin of 10 to 20 percentage points should be reserved based on the simulation results, and the performance gap can be narrowed through occupant training, regular maintenance, and intelligent control systems.

5.5.5. Future Research Directions

This study has several limitations that need to be overcome in future research. In terms of climate zone representation, only one city, Nanjing, was selected as a case study. Future research should expand to at least three different climate zones, such as severe cold regions, cold regions, and hot summer and warm winter regions, to compare the effectiveness boundaries of passive strategies in each climate zone. Regarding the diversity of building types, only six-story multi-story residential buildings were considered. Future research should include high-rise residential buildings, office buildings, schools, hospitals, etc. High-rise buildings face issues such as wind speed variation with height and limited window opening, while office buildings are used during the day and left vacant at night, so their passive strategies should focus on daytime heat dissipation rather than nighttime heat storage. In terms of cost–benefit analysis, only a rough payback period estimation was provided. Future research should establish a life-cycle cost model and a social cost–benefit model to quantify external benefits such as carbon emission reduction value, public health benefits from heat island mitigation, and savings in grid investment. Regarding dynamic adaptability, this study assumes that the strategies will operate continuously once installed, without considering the need for dynamic adjustment of strategy parameters in response to climate change trends. Future research should explore dynamic adaptive technologies such as adjustable shading systems, intelligent ventilation control, and variable reflectance exterior walls.

6. Conclusions

This study, set against the backdrop of the 2024 global record high temperatures and the doubling of heat-related mortality rates, addresses the systemic vulnerability of the adaptive feedback loop formed by active mechanical cooling, where air conditioning consumes electricity, intensifies the heat island effect, and further increases the cooling load. It proposes a passive emission pathway. The research focuses on optimizing heat exchange in building envelopes, aiming to reduce cooling loads, alleviate grid pressure, and enhance building resilience under extreme high temperatures without relying on new materials. A typical six-story multi-family residential building in the hot summer and cold winter climate zone of Nanjing was selected as a case study. Hourly simulations were conducted using EnergyPlus(V8.9), with 2024 high-temperature-corrected meteorological data as input, to compare the baseline building with three progressive passive strategies.

Three progressive passive strategy packages were designed, with Package A incorporating external shading and natural ventilation, Package B adding reflective coating and green roof, and Package C further adding night ventilation and high-performance windows. The load reduction effect and resilience improvement of each strategy were quantitatively analyzed through comparison of hourly simulation outputs.

The main research findings include four aspects. In terms of reducing cooling load, Package C achieved a peak load reduction rate of 62.5% and a seasonal total load reduction rate of 63.0% for the specific case study building. Regarding the transformation of heat exchange in the building envelope, Package C reduced the peak daytime heat gain from 68 watts per square meter to 22 watts and increased the nighttime heat loss from 12 watts per square meter to 38 watts. In terms of high-temperature resilience, under the condition of no active cooling on an extreme hot day of 41.2 degrees Celsius, the maximum indoor temperature was reduced from 36.8 degrees Celsius to 29.4 degrees Celsius, and the number of high-temperature risk hours was reduced from 782 h to 206 h. In terms of impact on the power grid, the peak power demand was reduced from 142 kilowatts to 42 kilowatts, and the system leverage factor was calculated as 1.08, meaning that for every 1-kilowatt reduction in building load, the modeled grid demand was reduced by 1.08 kilowatts under the assumed urban heat island feedback.

There are three research contributions. First, this study demonstrates that a load reduction exceeding 60% can be achieved using only mature and scalable passive design strategies without relying on new materials, indicating high feasibility for engineering practice under suitable conditions. Second, it introduces the concept of the systemic leverage effect to quantify the potential grid-level amplification of passive strategies through urban heat island mitigation. Third, it establishes a vulnerability-to-resilience transformation framework that clarifies the effectiveness boundaries and enabling conditions for passive strategies.

The findings are specific to the case study and should not be generalized to all net-zero futures. The reported effectiveness applies to Nanjing's hot summer and cold winter climate, and the performance of the passive strategies depends critically on several enabling conditions: a diurnal temperature range greater than 8 degrees Celsius to ensure effective night ventilation, favorable building orientation to maximize shading benefits, ambient noise below 60 decibels to allow for natural ventilation without acoustic discomfort, and acceptable outdoor air quality with PM2.5 below 75 micrograms per cubic meter during night ventilation hours. Future work should extend the framework to other climate zones including severe cold, cold, and hot summer and warm winter regions, develop a strategy matching matrix based on climate characteristics, diversify building types to include high-rise residential buildings, offices, schools, and hospitals, and explore dynamic adaptability technologies such as adjustable shading, intelligent ventilation, and variable reflectance exterior walls.

Supplementary Materials: The following supporting information can be downloaded at: https://www.mdpi.com/article/10.3390/buildings16132513/s1.

Author Contributions: Conceptualization, J.Z.; investigation, T.N.; formal analysis, J.Z. and H.W. methodology, J.Z. and G.S.; resources, T.N.; writing—review and editing, G.S. All authors have read and agreed to the published version of the manuscript.

Funding: The work described in this paper was supported by Undergraduate Innovation and Entrepreneurship Training Program Project of Jiangsu University of Science and Technology in 2024 (No. 202410289054Z); the Open Research Project of Anhui Province Key Laboratory of Intelligent Building & Building Energy Saving (No. IBES2025KF12); the Major Projects of Philosophical and Social Science Research in Universities in Jiangsu Province (No. 2023SJZD131).

Data Availability Statement: The original contributions presented in this study are included in the article/Supplementary Materials. Further inquiries can be directed to the corresponding author.

Conflicts of Interest: The authors declare no conflicts of interest.

References

1. Yasser, O.; Zahidi, I. Artificial intelligence for predicting urban heat island effect and optimising land use/land cover for mitigation: Prospects and recent advancements. *Urban Clim.* **2024**, *55*, 101976. [CrossRef]
2. Ramakreshnan, L.; Aghamohammadi, N. The Application of Nature-Based Solutions for Urban Heat Island Mitigation in Asia: Progress, Challenges, and Recommendations. *Curr. Environ. Health Rep.* **2024**, *11*, 4–17. [CrossRef] [PubMed]
3. Santamouris, M. Recent progress on urban overheating and heat island research. Integrated assessment of the energy, environmental, vulnerability and health impact. Synergies with the global climate change. *Energy Build.* **2020**, *207*, 109482. [CrossRef]
4. Xu, Y.; Vahmani, P.; Jones, A.; Hong, T. Anthropogenic heat from buildings in Los Angeles County: A simulation framework and assessment. *Sustain. Cities Soc.* **2024**, *107*, 105468. [CrossRef]
5. Sadeghi, F.; Najafi, N.; Pournasr, H. Multi-objective optimization of daylighting systems for energy efficiency and thermal-visual comfort in buildings: A review. *Build. Environ.* **2026**, *288*, 113921.
6. Mangkuto, R.A.; Koerniawan, M.D.; Paramita, B. Human-centric lighting in office spaces: Daylight strategies and environmental influences on visual effects and circadian health. *Build. Environ.* **2025**, *285*, 113538. [CrossRef]
7. Pathak, A.; Raj, A.P.; Ravikumar, R. A review on adaptive and non-adaptive shading devices for sustainable buildings. *J. Build. Eng.* **2024**, *95*, 110088.
8. Lare, Y.D.; Nougblega, Y.; Dowou, K.; Toka, A.K. Comparative Numerical study of the Thermal and Electrical Performance of Combined and Separated Solar Chimneys for Passive Space Cooling in Multi-Storey Buildings. *J. Fluid Flow Heat Mass Transf.* **2025**, *12*, 54–72. [CrossRef]
9. Jiao, K.; Lu, L.; Zhao, L.; Wang, G. Towards Passive Building Thermal Regulation: A State-of-the-Art Review on Recent Progress of PCM-Integrated Building Envelopes. *Sustainability* **2024**, *16*, 6482.
10. Li, M.; Shen, X.; Wu, W.; Cetin, K.; Mcintyre, F.; Wang, L.; Ding, L.; Bishop, D.; Bellamy, L.; Liu, M. Cooling demand reduction with nighttime natural ventilation to cool internal thermal mass under harmonic design-day weather conditions. *Appl. Energy* **2025**, *379*, 113963.
11. Junghans, L.; Kim, H. Evaluation of multiple predictive control strategies to optimally use building thermal mass to reduce annual operation costs and associated GHG emissions. *J. Build. Eng.* **2025**, *112*, 113963. [CrossRef]
12. Wang, L.; Ibrahim, A.; Jiang, Y. Multi-Objective Optimization of Atrium Form Variables for Daylighting, Energy Consumption and Thermal Comfort of Teaching Buildings at the Early Design Stage in Cold Climates. *Buildings* **2025**, *15*, 4434. [CrossRef]
13. Larasati, D.; Asawa, T.; Ferels, A.; Aisha, H.; Hanifah, Y. Enhancing Low-Cost Apartment Performance: A Comparative Study on Passive Design Implementation. *Int. J. Adv. Sci. Eng. Inf. Technol.* **2025**, *15*, 669–679.
14. Nie, Y.; Luo, M.; Liu, J.; Wu, Z. Assessment of passive climate-responsive strategies in vernacular Yinzi building: A case study in China's hot-summer and cold-winter climate. *Energy Build.* **2025**, *347*, 116274.
15. Li, E.; Zhang, X.; Chen, L.; Ma, W.; Li, S.; Zhang, M. Climate-responsive strategies in sunken courtyard cave dwellings: Architectural insights for modern passive design. *J. Asian Archit. Build. Eng.* **2025**, *24*, 1475–1500. [CrossRef]
16. Liu, Y. Sustainable passive design in cold regions: Energy and thermal evaluation of traditional Zhuangke dwellings in Qinghai Province, China. *Energy Build.* **2025**, *344*, 115969. [CrossRef]
17. Youssef, R.A.; Ayoub, M.; El-Khouly, T. Enhancing Visual Comfort and Energy Efficiency in Office Lighting Using Parametric-Generative Design Approach for Interactive Kinetic Louvers. *J. Daylighting* **2024**, *11*, 69–96. [CrossRef]
18. Liu, Y. Performance-Verified Classification of Vernacular Courtyard–Sunspace Configurations in Cold High-Radiation Regions. *Build. Environ.* **2026**, *297*, 114583.
19. Wu, Q. Active-passive coupling in building design: A review of parameter interactions for energy performance and thermal and visual comfort. *Energy Build.* **2026**, *356*, 117099. [CrossRef]
20. Sustainability Editorial Office. Climate-Adaptive Passive Design Strategies for Near-Zero-Energy Office Buildings in Central and Southern Anhui, China. *Sustainability* **2025**, *17*, 6535.
21. Liu, Y. Multiobjective optimisation of passive energy saving strategies in Zhuangke dwellings in Huangyuan county, China. *Sci. Rep.* **2025**, *15*, 26285. [CrossRef] [PubMed]
22. Han, F.; Wang, Y.; Feist, W.; Cao, X.; Yu, Z.; Song, B.; Benli, H.; Dermentzis, G. Exploring solutions to achieve carbon neutrality in China: A comparative study of a large-scale passive House district and a Green building district in Qingdao. *Energy Build.* **2022**, *268*, 112224. [CrossRef]
23. Xu, Z.; Zhang, X.; Yao, Y.; Chen, M. Superhydrophobic cement-based radiative cooling paint for durable and scalable applications. *Appl. Therm. Eng.* **2025**, *281*, 128770. [CrossRef]
24. Sui, Z.; Li, F.; Sui, Y.; Lin, H.; Wu, W. Ultra-high-flux passive cooling enabled by a sweating-inspired hygroscopic membrane. *Carbon Energy* **2025**, *7*, e665.
25. Ibrahim, A.; Alsukkar, M.; Dong, Y.; Saleem, F.; Hamza, A.; Hu, P.; Hu, M. Enhancing energy efficiency in shipping container house: A novel approach using hybrid louver systems. *Energy Built Environ.* **2024**, *7*, 278–294.

26. Yang, X.; Peng, L.L.H.; Jiang, Z.; Chen, Y.; Yao, L.; He, Y.; Xu, T. Impact of urban heat island on energy demand in buildings: Local climate zones in Nanjing. *Appl. Energy* **2020**, *260*, 114279. [CrossRef]
27. Liu, J.; Peng, C.H.; Zhang, J.X. Exploring influences of rural morphology on building cluster energy consumption and retrofit performance: A case study of Nanjing, China. *Build. Environ.* **2025**, *284*, 113427. [CrossRef]
28. Huang, Y.; Akbari, H.; Taha, H.; Rosenfeld, A.H. The potential of vegetation in reducing summer cooling loads in residential buildings. *J. Appl. Meteorol. Climatol.* **1987**, *26*, 1103–1116. [CrossRef]
29. Kim, K.A.; Park, K.H. Temperature change in building layers according to cool roofs application: A case study at Changwon National University. *KIEAE J.* **2018**, *18*, 103–111. [CrossRef]
30. Xu, F.; Zhang, J.; Gao, Z. A case study of the effect of building surface cool and super cool materials on residential neighbourhood energy consumption in Nanjing. *Renew. Sustain. Energy Rev.* **2024**, *189*, 114027.

Disclaimer/Publisher's Note: The statements, opinions and data contained in all publications are solely those of the individual author(s) and contributor(s) and not of MDPI and/or the editor(s). MDPI and/or the editor(s) disclaim responsibility for any injury to people or property resulting from any ideas, methods, instructions or products referred to in the content.